Parasitol Res
DOI 10.1007/s00436-011-2677-9

SHORT COMMUNICATION

A novel C-type lectin identified by EST analysis in tissue migratory larvae of *Ascaris suum*

Ayako Yoshida · Eiji Nagayasu · Yoichiro Horii · Haruhiko Maruyama

Received: 19 July 2011 / Accepted: 30 September 2011

Abstract C-type lectins (CTLs) are a group of proteins which bind to carbohydrate epitopes in the presence of Ca^{2+}, which have been described in a wide range of species. In this study, a cDNA sequence coding a putative CTL has been identified from the cDNA library constructed from the pig round worm *Ascaris suum* lung L3 (LL3) larvae, which was designated as *A. suum* C-type lectin-1 (As-CTL-1). The 510 nucleotide open reading frame of As-CTL-1 cDNA encoded the predicted 169 amino acid protein including a putative signal peptide of 23 residues and C-type lectin/C-type lectin-like domain (CLECT) at residue 26 to 167. As-CTL-1 was most similar to *Toxocara canis* C-type lectin-1 and 4 (*Tc*-CTL-1 and 4), and highly homologous to namatode CTLs and mammalian CTLs as well, such as human C-type lectin domain family 4 member G (CLECG4). In addition, As-CTL-1 was strongly expressed in tissue migrating LL3 and the L4 larvae, which were developmental larvae stages within the mammalian host. These results suggest that *A. suum* larvae might utilize As-CTL-1 to avoid pathogen recognition mechanisms in mammalian hosts due to it is similarity to host immune cell receptors.

A. Yoshida (✉) · E. Nagayasu · H. Maruyama
Department of Infectious Diseases, Division of Parasitology,
Faculty of Medicine, University of Miyazaki,
5200 Kihara, Kiyotake,
Miyazaki 889-1692, Japan
e-mail: kukuri@med.miyazaki-u.ac.jp

Y. Horii
Laboratory of Veterinary Parasitic Diseases,
Department of Veterinary Sciences, Faculty of Agriculture,
University of Miyazaki,
Miyazaki, Japan

Published online: 18 October 2011

Introduction

C-type lectins (CTLs) constitute a large family of proteins that binds carbohydrate moieties in a Ca^{2+}-dependent manner (Drickamer 1988, 1996). They are characterized by a conserved C-type lectin/C-type lectin-like domain (CLECT) which shares Ca^{2+}- and carbohydrate-binding motifs. CLECT also contains at least four critical cysteine residues which form a two-loop structure by disulphide bounds. It is well known that CTLs are widely expressed among metazoan organisms (Drickamer and Fadden 2002; Zelensky and Gready 2005). In vertebrates, CTL represents a very large family that is classified into 17 groups (Drickamer and Fadden 2002), many of which are known as pattern-recognition receptors implicated in the recognition of pathogens by innate immunity (Weis et al. 1998). In addition, some evidence have indicated that CTLs play an important role in immune homeostasis by endogenous 'self' ligand recognition (García-Vallejo and van Kooyk 2009), and they themselves have a bactericidal activation (Cash et al. 2006).

Ascaris suum, a common round worm in pigs, is infective to a wide range of hosts, including humans, mice, cattle and chickens. When embryonated eggs are ingested by a definitive swine host, larvae hatch in the small intestine, penetrate the intestinal mucosa, and migrate through the liver and lungs, before finally reaching the intestine, where they sexually mature and produce eggs (Dold and Holland 2011). In contrast, it is generally considered that larvae, which are reached the lungs following liver migration, disperse into various tissues and

organs without further development in non-swine host (Slotved et al. 1998; Crompton 2001), although *A. suum* has been reported to develop into adult stage infrequently in human hosts (Anderson 1995; Nejsum et al. 2005; Arizono et al. 2010). However, it has not been fully explained how they discriminate pigs and other animals and what kind of interaction is involved between host and parasite during the lung phase of migration.

Expressed sequencing tag (EST) analysis is a powerful tool for profiling the gene expression pattern in a particular parasite population. Although publicly available EST databases of *A. suum* already exist in NAMBASE4 (http://www.nematodes.org/nembase4/index.shtml), they were constructed from adult worm, intestinal L4 larvae, newly hatched infective larvae (iL3) and egg embryos. EST analysis of tissue-migrating larvae has not yet been performed. Therefore, we explored cDNA of *A. suum* lung L3 (LL3) collected from infected rabbit lungs in order to examine what kind of biological processes were activated in tissue-migrating larvae. As one of the most frequently occurring clones, we identified a cDNA sequence for a putative *A. suum* CTL that showed specific expression during internal larval stages in mammalian hosts.

Materials and methods

Parasites and infection

Adult *A. suum* were collected from infected pigs at a local abattoir in Japan. Eggs were freed from the uterine tissue by incubating uteri in 0.1 N NaOH. After washing with distilled water, eggs were suspended and stirred in 0.1 N H_2SO_4 and cultured at 27°C for 3–4 weeks. Infective L3 larvae (iL3) were mechanically hatched from eggs and isolated free from egg shell contaminants (Takamiya et al. 1993). For the preparation of lung L3 larvae, male Japanese white rabbits (Kyudo, Kumamoto, Japan) were orally inoculated with 1.5×10^5 embryonated eggs. Six days after infection, the lungs were removed and cut into 5-mm cubes using scissors. The cubes were wrapped with Kimwipe papers and incubated in phosphate-buffered saline (PBS) at 37°C for 1.5 h, and then emerging worms were collected. Culture driven-L4 larvae (cL4) were obtained from cultures of LL3 in vitro (Islam et al. 2006).

RNA isolation and cDNA library construction

Total RNA of LL3 was isolated with TRIzol Reagent (Invitrogen, Carlsbad, CA), followed by purification of poly $(A)^+$ RNA with GenElute™ mRNA Miniprep Kit (Sigma, St. Louis, MO). A cDNA library was constructed using the SMART cDNA Library Construction Kit (Clontech, Mountain View, CA). The reverse transcription step was performed using MMLV Reverse Transcriptase with the SMART IV oligonucleotide primer and the CDS III/3′ PCR primer provided in the kit. The double-stranded cDNA (ds-cDNA) was synthesized by long distance PCR with the 5′ PCR primer and the CDS III/3′ PCR primer using the Advantage 2 PCR kit (Clontech). The ds-cDNA was treated with proteinase K and then digested by *Sfi*I. After size fractionation, cDNA was cloned into pDNR-LIB vector, and transformed into *Escherichia coli* ElectroMAX™ DH10B™ cells (Invitrogen, Carlsbad, CA).

EST sequencing, processing and analysis

Plasmid DNA of the 2,024 randomly selected clones was extracted and single-pass sequenced from the 5′-end using sequencing primer (5′-GCATACATTATACGAAGTTAT CAGTCG-3′). The sequencing was conducted on an ABI Prism 3130xl Genetic Analyzer (Applied Biosystems, Carlsbad, CA), using ABI Prism Big-Dye Terminator v3.1 Cycle Sequencing Kit (Applied Biosystems). EST sequences were clustered using SEQUENCHER (Gene Codes Corporation, Ann Arbor, MI), with a minimum sequence overlap length cut-off of 30 bases and an identity threshold of 90%, for the removal of flaking vector and adaptor sequences, followed by assembly. These contigs and singletons were subjected to BLASTN and BLASTX programs (E value of $\leq1\times10^{-5}$) at the National Center for Biotechnology Information (http://blast.ncbi.nlm.nih.gov/Blast.cgi). A protein sequence motif was identified using the InterProScan at The European Bioinformatics Institute (Zdobnov and Apweiler 2001). Alignment of ESTs was conducted by using GENETYX-WIN software (Genetyx Corporation, Tokyo, Japan).

Real-time PCR analysis

Total RNA from iL3, LL3, cL4 and adult worm tissues (head, muscle, intestine, uterus, ovary and testis) was extracted with TRIzol reagent. After treatment with DNaseI (Ambion Inc., Austin, TX), cDNA was generated from 250 ng of total RNA using PrimeScript® 1st strand cDNA Synthesis Kit (Takara Bio Inc., Shiga, Japan). Primer sets for amplification were as follows: As CTL-1 (sense, 5′-CCACCATGTTCTCGACCGTTGCT-3′; antisense, 5′-ATTTCCTCCTACTGGCGCTCCT-3′) and 18S ribosomal RNA gene (sense, 5′-ATCGGTCGCGTAGGGTGGCT-3′; antisense, 5′-AAGCCGCAGGCTCCACTCCT-3′). Real-time PCR was then performed with an ABI Prism 7000 Sequence Detection Systems (Applied Biosystems) and a GoTaq® qPCR Master Mix (Promega, Madison, WI). Relative quantification was assessed by normalizing the amount of the target transcript to the 18S ribosomal RNA gene.

Results and discussion

In paratenic hosts such as humans, larvae of *A. suum* penetrate the mucosal epithelium but thereafter remain developmentally arrested in the migratory tissue phase (Crompton 2001). To understand biological events taking place in the arrested larvae, we carried out EST analysis in a cDNA library of migrating L3 larvae (LL3) collected from infected rabbit lungs (LL3). As a result from 5′ ends single-pass sequencing of 2,024 clones, 1,650 ESTs were yielded. Upon clustering, these ESTs were represented by 279 distinct gene products, which consist of 78 contigs and 201 singletons.

The consensus sequences of contigs and singletons were compared against NCBI BLAST databases in BLASTX analysis, revealing a novel CTL sequence referred to as *A. suum* C-type lectin-1 (As-CTL-1). We focused on this molecule, because CTL might contribute to the establishment of successful parasitism in nematodes (Loukas et al. 1999; Urwin et al. 2002). Using RT-PCR, the full-length cDNA corresponding to As-CTL-1 was successfully amplified from LL3 RNA (data not shown). As-CTL-1 is 710 nucleotides (GenBank accession no. HQ025087), which encoded the protein of 169 amino acids including the putative signal peptide of 23 residues and C-type lectin/C-type lectin-like domain (CLECT) at residue 26 to 167. The four cysteine residues at positions 62, 136, 154 and 166, which are required to form the CLECT internal disulfide bridge formations (Zelensky and Gready 2003), were completely conserved in As-CTL-1, but the WIGL and WND motifs conserved in the classical CTLs (Zelensky and Gready 2003) were replaced by WLAL and WDD. According to carbohydrate specificity, CTLs are categorized into mannose/GlcNAc - or galactose/GalNAc -recognizing lectins (Weis et al. 1992; Iobst and Drickamer 1994). These differences suggest substitutions at the key substrate binding residues. As-CTL-1 had QPD, which was found in galactose/GalNAc-binding CTLs. Thus, although the Ca^{2+}-dependent carbohydrate binding activity of As-CTL-1 was not assessed in this study, it is most likely a galactose-binding CTL from its amino acid motifs.

Subsequent sequence analysis showed that the amino acid sequence of CLECT in As-CTL-1 was found to have 33% identity to canine roundworm *Toxocara canis* C-type lectin-1 (*Tc*-CTL-1) and 38% identity to *Tc*-CTL-4. It has been reported that the free-living nematode *Caenorhabditis elegans* has more than 270 genes encoding CLECT of CTLs in their genome (Schulenburg et al. 2008). Interestingly, As-CTL-1 showed greater identity with human CTL domain family 4 member G (CLECG4; 28% identity) than with the *C. elegans* homologue (clec-149; 24% identity). Considering the eukaryotic phylogeny, it is reasonable that several CTLs from parasitic nematodes, such as *Ancylostoma ceylanicum* (AceCTL-1), *Necator americanus* (NaCTL-2), *Heligmosomoides polygyrus* (*Hp*-CTL-1) and *Nippostrongylus brasiliensis* (*Nb*-CTL-1 and 2) CTLs, share greater identity with *C. elegans* CTLs than mammalian CTLs (Brown et al. 2006; Daub et al. 2000; Harcus et al. 2009). On the other hand, *Tc*-CTL-1, *Tc*-CTL-4 and NaCTL-1, as well as As-CTL-1, appear to be much closer to homologues in mammalian CTLs than those in *C. elegans* (Loukas et al. 1999, 2000; Daub et al. 2000), raising speculations about the role they might play in the adaptation to parasitism.

The expression of As-CTL-1 was evaluated by real-time PCR in different developmental stages, including mechanically hatched iL3, LL3, cL4 and adult (Fig. 1). The mRNA for As-CTL-1 was scarcely detected in iL3 and tissues from adult worms, including the head, muscle, intestine, uterus, ovary and testis, whereas LL3 and cL4 larvae showed strong expression of As-CTL-1 transcript. After arriving at the jejunum, L3 larvae developed to L4 stage larvae in definitive swine host in vivo. These results indicate that the expression of As-CTL-1 is up-regulated through the tissue migrating stage and intestinal larval stage.

Although the physiological function of CTLs remains unclear, a number of nematode CTLs identified so far act as a pathogen recognition molecule or an antibacterial protein in immune responses to protect the worm itself against microbial infection (O'Rourke et al. 2006; Schulenburg et al. 2008). However, considering that the expression of As-CTL-1 is confined during tissue migration, it would not be very likely that As-CTL-1 is employed for the recognition of microbes in *A. suum*, because the worms may not encounter hazardous bacteria on the migrating route, which would be maintained clean by the host immunity. Instead, greater sequence identity that As-CTL-1 shares with mammalian CTLs than *C. elegans* proteins, seems to suggest that As-CTL-1 acts as a

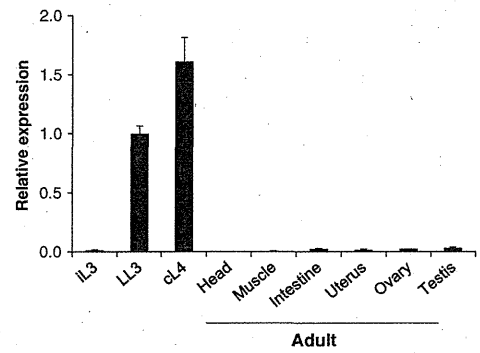

Fig. 1 Comparison of As-CTL-1 mRNA expression in developmental stages. Real-time PCR was performed with mechanically hatched iL3, LL3, cL4 and various adult worm tissues (head, muscle, intestine, uterus, ovary and testis). Relative expression of the As-CTL-1 mRNA was assessed by normalizing to 18S rRNA expression. Data were expressed as a ratio to As-CTL-1 gene expression in LL3

competitor for host cell receptors, possibly interfering host immune response to the worms (Loukas and Maizels 2000; Loukas and Prociv 2001). As-CTL-1 might be able to bind to ligands for mammalian CTL, such as NK receptors and/or macrophage/dendritic cell receptors (Osorio and Reis e Sousa 2010; Sun and Lanier 2011). In the present study, As-CTL-1 showed high similarity to *Tc*-CTLs and specific expression in LL3 and cL4, both of which were exposed to attack by host immune responses. Considering these findings, *A. suum* larvae might interfere with host inflammation processes by As-CTL-1 to avoid protective immune responses in infected animals during tissue migration. Further study on functional aspects of this molecule will identify novel dimensions of the host–parasite relationship and the significance of tissue migration in ascarid infection.

Acknowledgements We thank Hisako Kyan and Naomi Takeda for providing *A. suum* adult worm. This work was supported by grants from the Ministry of Education, Culture, Sports, Science and Technology of Japan (Grant-in-Aid for Scientific Research C 21590466, Grant-in-Aid for Scientific Research on Priority Areas 'Matrix of Infection Phenomena' 21022041), the Ministry of Health, Labour and Welfare (H23-Shinko-Ippan-014, H23-Kokui-Shitei- 003, H22-Seisakusouyaku-Ippan-003) and grants from the University of Miyazaki (Support Program for Female Researchers M41D1123 and Integrated Research Project for Human and Veterinary Medicine).

References

Anderson TJC (1995) Ascaris infections in humans from North America: molecular evidence for cross-infection. Parasitology 110(2):215–219

Arizono N, Yoshimura Y, Tohzaka N, Yamada M, Tegoshi T, Onishi K, Uchikawa R (2010) Ascariasis in Japan: is pig-derived *Ascaris* infecting humans? Jpn J Infect Dis 63(6):447–448

Brown AC, Harrison LM, Kapulkin W, Jones BF, Sinha A, Savage A, Villalon N, Cappello M (2006) Molecular cloning and characterization of a C-type lectin from *Ancylostoma ceylanicum*: evidence for a role in hookworm reproductive physiology. Mol Biochem Parasitol 151(2):141–147

Cash HL, Whitham CV, Behrendt CL, Hooper LV (2006) Symbiotic bacteria direct expression of an intestinal bactericidal lectin. Science 313(5790):1126–1130

Crompton DW (2001) Ascaris and ascariasis. Adv Parasitol 48:285–375

Daub J, Loukas A, Pritchard DI, Blaxter M (2000) A survey of genes expressed in adults of the human hookworm, *Necator americanus*. Parasitology 120(2):171–184

Dold C, Holland CV (2011) Ascaris and ascariasis. Microbes Infect 13 (7):624–631

Drickamer K (1988) Two distinct classes of carbohydrate-recognition domains in animal lectins. J Biol Chem 263(20):9557–9560

Drickamer K (1996) Ca(2+)-dependent sugar recognition by animal lectins. Biochem Soc Trans 24(1):146–150

Drickamer K, Fadden AJ (2002) Genomic analysis of C-type lectins. Biochem Soc Symp 69:59–72

García-Vallejo JJ, van Kooyk Y (2009) Endogenous ligands for C-type lectin receptors: the true regulators of immune homeostasis. Immunol Rev 230(1):22–37

Harcus Y, Nicoll G, Murray J, Filbey K, Gomez-Escobar N, Maizels RM (2009) C-type lectins from the nematode parasites *Heligmosomoides polygyrus* and *Nippostrongylus brasiliensis*. Parasitol Int 58(4):461–470

Iobst ST, Drickamer K (1994) Binding of sugar ligands to Ca(2+)-dependent animal lectins: II. Generation of high-affinity galactose binding by site-directed mutagenesis. J Biol Chem 269 (22):15512–15519

Islam MK, Miyoshi T, Yamada M, Alim MA, Huang X, Motobu M, Tsuji N (2006) Effect of piperazine (diethylenediamine) on the moulting, proteome express and pyrophosphate activity of *Ascaris suum* lung-stage larvae. Acta Trop 99:208–217

Loukas A, Mullin NP, Tetteh KK, Moens L, Maizels RM (1999) A novel C-type lectin secreted by a tissue-dwelling parasitic nematode. Curr Biol 9(15):825–828

Loukas A, Maizels RM (2000) Helminth C-type lectins and host–parasite interactions. Parasitol Today 16(8):333–339

Loukas A, Doedens A, Hintz M, Maizels RM (2000) Identification of a new C-type lectin, TES-70, secreted by infective larvae of *Toxocara canis*, which binds to host ligands. Parasitology 121 (5):545–554

Loukas A, Prociv P (2001) Immune responses in hookworm infections. Clin Microbiol Rev 14:689–703

Nejsum P, Parker ED Jr, Frydenberg J, Roepstorff A, Boes J, Haque R, Astrup I, Prag J, Skov Sørensen UB (2005) Ascariasis is a zoonosis in Denmark. J Clin Microbiol 43(3):1142–1148

O'Rourke D, Baban D, Demidova M, Mott R, Hodgkin J (2006) Genomic clusters, putative pathogen recognition molecules, and antimicrobial genes are induced by infection of *C. elegans* with *M. nematophilum*. Genome Res 16(8):1005–1016

Osorio F, Reis e Sousa C (2010) Myeloid C-type lectin receptors in pathogen recognition and host defense. Immunity 34(5):651–664

Schulenburg H, Hoeppner MP, Weiner J 3rd, Bornberg-Bauer E (2008) Specificity of the innate immune system and diversity of C-type lectin domain (CTLD) proteins in the nematode *Caenorhabditis elegans*. Immunobiology 213(3–4):237–250

Slotved HC, Eriksen L, Murrell KD, Nansen P (1998) Early *Ascaris suum* migration in mice as a model for pigs. J Parasitol 84(1):16–18

Sun JC, Lanier LL (2011) NK cell development, homeostasis and function: parallels with CD8+ T cells. Nat Rev Immunol 11:645–657

Takamiya S, Kita K, Wang H, Weinstein PP, Hiraishi A, Oya H, Aoki T (1993) Developmental changes in the respiratory chain of *Ascaris* mitochondria. Biochim Biophys Acta 1141:65–74

Urwin PE, Lilley CJ, Atkinson HJ (2002) Ingestion of double-stranded RNA by preparasitic juvenile cyst nematodes leads to RNA interference. Mol Plant Microbe Interact 15(8):747–752

Weis WI, Drickamer K, Hendrickson WA (1992) Structure of a C-type mannose-binding protein complexed with an oligosaccharide. Nature 360(6400):127–134

Weis WI, Taylor ME, Drickamer K (1998) The C-type lectin superfamily in the immune system. Immunol Rev 163:19–34

Zdobnov EM, Apweiler R (2001) InterProScan – an integration platform for the signature-recognition methods in InterPro. Bioinformatics 17:847–848

Zelensky AN, Gready JE (2003) Comparative analysis of structural properties of the C-type-lectin-like domain (CTLD). Proteins 52:466–477

Zelensky AN, Gready JE (2005) The C-type lectin-like domain superfamily. FEBS J 272(24):6179–6217

Biochimica et Biophysica Acta 1820 (2012) 643–651

Contents lists available at SciVerse ScienceDirect

Biochimica et Biophysica Acta

journal homepage: www.elsevier.com/locate/bbagen

Review

Mitochondrial fumarate reductase as a target of chemotherapy: From parasites to cancer cells☆

Chika Sakai [a], Eriko Tomitsuka [a,b], Hiroyasu Esumi [b], Shigeharu Harada [c], Kiyoshi Kita [a,*]

[a] Department of Biomedical Chemistry, Graduate School of Medicine, The University of Tokyo, Tokyo 113-0033, Japan
[b] Cancer Physiology Project, Investigative Treatment Division, National Cancer Center Research Institute East, 6-5-1 Kashiwanoha, Kasiwa, Chiba 277-8577, Japan
[c] Department of Applied Biology, Graduate School of Science and Technology, Kyoto Institute of Technology, Kyoto 606-8585, Japan

ARTICLE INFO

Article history:
Received 27 July 2011
Received in revised form 28 November 2011
Accepted 17 December 2011
Available online 29 December 2011

Keywords:
Mitochondrial fumarate respiration
Complex II
Hypoxia
Drug target
Ascaris suum
Type II flavoprotein subunit

ABSTRACT

Recent research on respiratory chain of the parasitic helminth, *Ascaris suum* has shown that the mitochondrial NADH-fumarate reductase system (fumarate respiration), which is composed of complex I (NADH–rhodoquinone reductase), rhodoquinone and complex II (rhodoquinol–fumarate reductase) plays an important role in the anaerobic energy metabolism of adult parasites inhabiting hosts. The enzymes in these parasite-specific pathways are potential target for chemotherapy. We isolated a novel compound, nafuredin, from *Aspergillus niger*, which inhibits NADH-fumarate reductase in helminth mitochondria at nM order. It competes for the quinone-binding site in complex I and shows high selective toxicity to the helminth enzyme. Moreover, nafuredin exerts anthelmintic activity against *Haemonchus contortus* in *in vivo* trials with sheep indicating that mitochondrial complex I is a promising target for chemotherapy. In addition to complex I, complex II is a good target because its catalytic direction is reverse of succinate–ubiquinone reductase in the host complex II. Furthermore, we found atpenin and flutolanil strongly and specifically inhibit mitochondrial complex II.
Interestingly, fumarate respiration was found not only in the parasites but also in some types of human cancer cells. Analysis of the mitochondria from the cancer cells identified an anthelminthic as a specific inhibitor of the fumarate respiration. Role of isoforms of human complex II in the hypoxic condition of cancer cells and fetal tissues is a challenge. This article is part of a Special Issue entitled Biochemistry of Mitochondria, Life and Intervention 2010.

1. Introduction

In the general understanding of bioenergetics of higher eukaryotes, oxygen is a most important terminal electron acceptor of mitochondrial respiratory chain (Fig. 1). The major function of the aerobic respiratory chain is the electrogenic translocation of protons out of the mitochondrial or bacterial membrane to generate the proton motive force that drives ATP synthesis by F_oF_1-ATPase. This mechanism of oxidative phosphorylation is conserved basically from aerobic bacteria to human mitochondria. However, recent study on the respiratory chain of the lower eukaryotes which reside micro-aerophilic environment has shown that the mitochondrial NADH-fumarate reductase system (fumarate respiration) plays an important role in the anaerobic energy metabolism [1]. This system is composed of complex I (NADH-quinone reductase), low potential quinone species and complex II (quinol–fumarate reductase: QFR).

Fumarate respiration is well known electron transport chain in the anaerobic bacteria [2]. Reducing equivalent of NADH is transferred to low potential quinone such as naphthoquione by complex I and finally is oxidized by fumarate by the fumarate reductase activity of complex II which is a reverse reaction of succinate–ubiquinone reductase (SQR) activity of complex II. By using this respiratory chain, bacteria are able to synthesize ATP even in the absence of oxygen. Recently our study of parasitic nematode, *Ascaris suum*, showed fumarate respiration also plays an important role in the anaerobic energy metabolism of adult worms, which reside in the host small intestine where oxygen tension is low [1]. Although fumarate reductase activities of bacterial and mitochondrial complex IIs are the same reaction, evolutional positions of each enzyme are quite different. All four subunits of complex II in adult *A. suum* are more closely related to the bacterial and mitochondrial SQR than to bacterial QFR [3–5].

Abbreviations: FRD, fumarate reductase; L3, 3rd stage larvae; LL3, lung stage L3; MK, menaquinone; SDH, succinate dehydrogenase; SQR, succinate–ubiquinone reductase; TCA cycle, tricarboxylic acid cycle; QFR, quinol–fumarate reductase; RQ, rhodoquinone

☆ This article is part of a Special Issue entitled Biochemistry of Mitochondria, Life and Intervention 2010.

* Corresponding author at: Department of Biomedical Chemistry, Graduate School of Medicine, The University of Tokyo, Hongo, Bunkyo-ku, Tokyo 113-0033, Japan. Tel.: +81 3 5841 3526; fax: +81 3 5841 3444.
E-mail address: kitak@m.u-tokyo.ac.jp (K. Kita).

0304-4165/$ – see front matter © 2011 Elsevier B.V. All rights reserved.
doi:10.1016/j.bbagen.2011.12.013

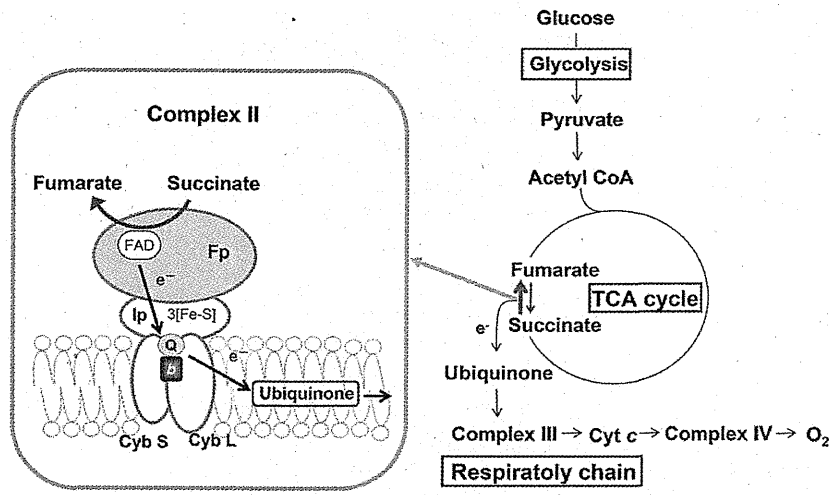

Fig. 1. Complex II is the member of TCA cycle and respiratory chain.Complex II catalyzes the oxidation of succinate to fumarate in the TCA cycle and transports the electron generated by this oxidation to ubiquinone in the respiratory chain. Generally, complex II consists of four subunits. Flavoprotein (Fp) subunit contains a flavin adenine dinucleotide prosthetic group and iron–sulfur protein (Ip) subunit contains three iron–sulfur clusters. There are two hydrophobic cytochrome*b* (Cyb L, Cyb S) subunits. The succinate binding site is located in Fp subunit, while the quinone binding site is formed by three subunits, Ip, Cyb L and CybS. Complex II also catalyzes the reduction of fumarate, a reverse-reaction of succinate dehydrogenase, in the respiratory chain of mitochondria from anaerobic animals, such as *Ascaris suum*, as well as anaerobic bacteria.

Thus, mitochondrial QFR is a new enzyme evolved by "reverse evolution" of SQR rather than direct evolution from bacterial QFR [6].

Recently our study has revealed that fumarate respiration functions in some human cancer cells and supports a survival of cancer cells in low nutrition and low oxygen conditions [7,8]. Furthermore, we found complex II with high QFR activity produces reactive oxygen species (ROS) [9]. ROS has been reported to contribute to proliferation and metastasis of cancer cells via the stabilization of hypoxia-inducible factor-1 (HIF-1) [10]. In addition, succinate produced by fumarate respiration also stabilize HIF-1 by the product inhibition of HIF prolyl hydroxylase, which catalyzes the oxygen-dependent hydroxylation of the conserved proline residues in HIF-1 α [11]. Thus, the relationship between accumulation of succinate resulted from functional defect of human complex II by the mutation of the subunits and carcinogenesis has recently become a focus of research [8].

As fumarate respiration is essential for the growth and survival of the parasites and some cancer cells, it should be a promising target of chemotherapy for both parasitic diseases and cancer. In this review, we focus on recent advances in the study of parasite and human mitochondrial fumarate respiration and complex II which is an important component of the system [8].

2. Fumarate respiration of parasite mitochondria

2.1. Life cycle of *A. suum* and changes in respiratory chain

A. suum is the most widely known parasite, and has been studied as a representative of human and livestock parasites [12–14]. Because of its large size, *A. suum* is ideal for the study including biochemical analysis. Adult *A. suum* resides in the small intestine of mammals, and the female produces between 200,000 and 400,000 fertilized eggs per day (Fig. 2). Eggs are excreted with feces and become mature eggs containing infectious 3rd stage larvae (L3) in about 2–3 weeks at normal temperature. The eggs reach the small intestine and hatch, when orally ingested by a host. A hatched larva invades the intestinal wall, and migrates to the liver, lung, trachea, and pharyngeal region, and finally returns to the intestine via the esophagus and stomach, and becomes an adult worm. In humans, the larvae of *A. suum* migrate to several organs including liver and lung and cause a wide variety of nonspecific symptoms such as general malaise, cough, liver dysfunction, hypereosinophilia with hepatomegaly and/or pneumonia. The oxygen concentration of the small intestine (~5%) is approximately 25% of that outside the body, and provides an environment of low oxygen tension in which the energy metabolism of the adult differs considerably from that of the larvae and the host (Fig. 3). The phosphoenolpyruvate carboxykinase (PEPCK)–succinate pathway, an anaerobic glycolytic pathway, operates in the adult worm, producing ATP under such a hypoxic conditions. This system is used by many other parasites such as *Echinococcus multilocularis* [15], and has also been observed in the adductor muscle of oysters and other bivalves that require energy conversion under anaerobic conditions. It is therefore considered to be a very common pathway for energy metabolism in adaptation to hypoxic environment [16,17].

The first half of the PEPCK–succinate pathway is the same glycolytic pathway found in mammals, in which phosphoenolpyruvate (PEP) is produced. In contrast to aerobic metabolism in mammals involving the conversion of PEP to pyruvate by pyruvate kinase, the *A. suum* adult fixes CO_2 with PEPCK to produce oxaloacetate (OAA). The OAA is converted to malate by the reverse reaction of malate dehydrogenase and transported into the mitochondria to produce pyruvate and fumarate. The NADH formed during production of pyruvate from malate is used in the reduction of fumarate to succinate. The NADH-fumarate reductase system, which is the anaerobic electron transport system characteristic of adult *A. suum* mitochondria, is the final step of this pathway. Unique property of this pathway is discussed in the next section.

In contrast to larvae which require oxygen for their development and possess the respiratory system to be almost the same as that of mammals, cytochrome *c* oxidase (complex IV) is not found in the respiratory chain of adult *A. suum* mitochondria, and the content of ubiquinol–cytochrome *c* reductase complex (complex III) is extremely low [18]. In addition to the enzymes, quinone species in the mitochondria also change during the life cycle of *A. suum*. In contrast to adult mitochondria, in which the low-potential rhodoquinone (RQ; $Em' = -63mV$) is the major quinone, ubiquinone (UQ; $Em' = +110mV$) is the major quinone of larvae (Fig. 4A) [19]. A combination of SQR and UQ, and that of QFR and a low-potential quinone, such as RQ or menaquinone (MK), is also observed in *Escherichia coli* and other bacteria during metabolic adaptation to changes in

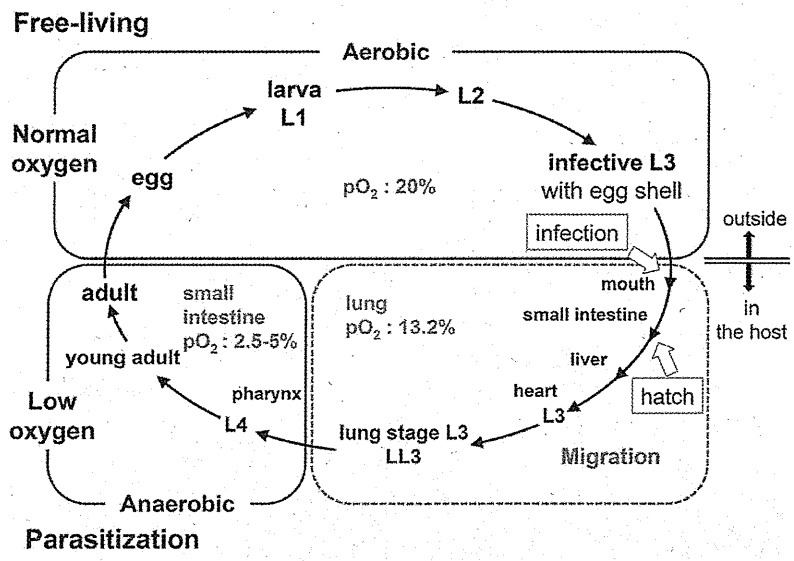

Fig. 2. Life cycle of *Ascaris suum*.Fertilized eggs grow to be infective L3 under aerobic environment. Infective L3 larvae are ingested by the host, reach the small intestine and hatch there. Afterwards, larvae migrate into host body (liver, heart, lung, pharynx), and finally migrate back to the small intestine and become adults. In the host small intestine, the oxygen concentration is low (pO_2=2.5–5%) compared with the exogenous environment (pO_2=20%). The metabolic pathway of *A. suum* changes dramatically during its life cycle, to adapt to changes in the environmental oxygen concentration [6].

oxygen supply [20,21]. Lower potential of RQ and MK is favorable for the electron transfer from NADH to fumarate (Fig. 4B). In this way, UQ participates in aerobic metabolism in *A. suum* larva, whereas RQ participates in anaerobic metabolism in adult *A. suum*.

Although studies have shown a clear difference in energy metabolism between larval and adult *A. suum* mitochondria, little is known about changes in the properties of mitochondria during migration of *A. suum* larvae in the host. As described later, examination of the changes in enzymatic characteristics and subunit composition of *A. suum* larval complex II from lung stage L3 (LL3) larvae obtained from rabbits showed that properties of LL3 mitochondria differed from those of L3 and adult mitochondria [22]. Protein chemical analysis revealed that the change in complex II begins with the anchor subunit, and then occurs in the catalytic subunit. Thus, *A. suum* is able to adapt to changes in oxygen concentration in the environment during its life cycle by dynamic change of respiratory chain.

2.2. NADH-fumarate reductase system (fumarare respiration) of *A. suum* adult

The final step of the PEPCK–succinate pathway, which plays such an important role in the anaerobic energy metabolism of the *A. suum* adult, is catalyzed by the NADH-fumarate reductase system as

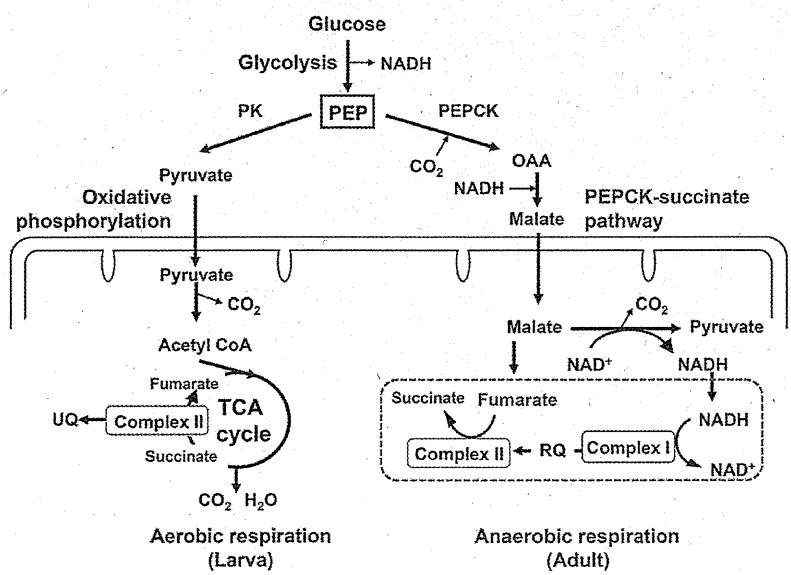

Fig. 3. Glucose metabolism of *A. suum* larval and adult mitochondria.The metabolic pathway of *A. suum* adult has a unique anaerobic electron transport system, NADH-fumarate reductase system. In the phospho*enol*pyruvate carboxykinase (PEPCK)–succinate pathway, phospho*enol*pyruvate (PEP) produced by a glycolytic process is carboxylated to form oxaloacetate and is then reduced to malate. The cytosolic malate is transported into the mitochondria, where it is first reduced to fumarate, and finally to succinate by the rhodoquinol–fumarate reductase activity of complex II. The terminal step is catalyzed by the NADH-fumarate reductase system (boxed in broken lines) comprised of complex I, rhodoquinone (RQ), and complex II. PEP, phosphoenolpyuvate; PEPCK, phoshoenolpyruvate carboxykinase; OAA, oxaloacete [6].

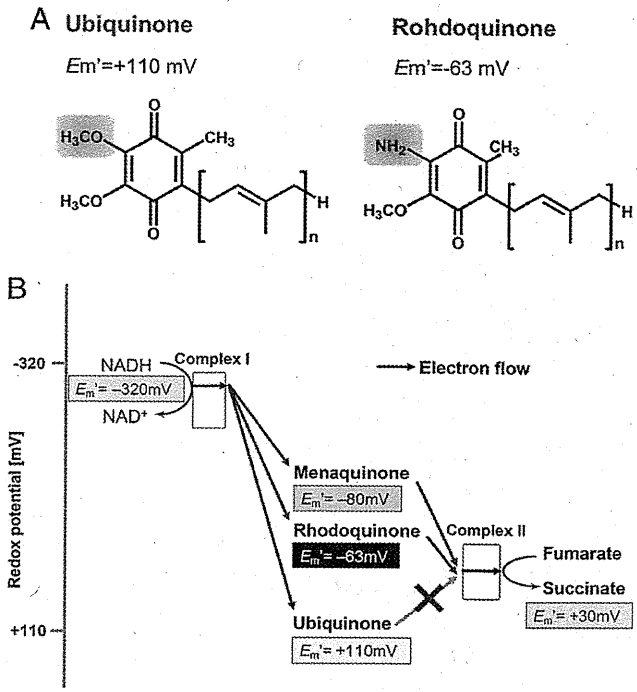

Fig. 4. Chemical structure and redox potentials of the quinones. A. Chemical structures of UQ and RQ. n, numbers of isoprenyl groups in side-chain. B. Redox potentials of quinones and substrates.

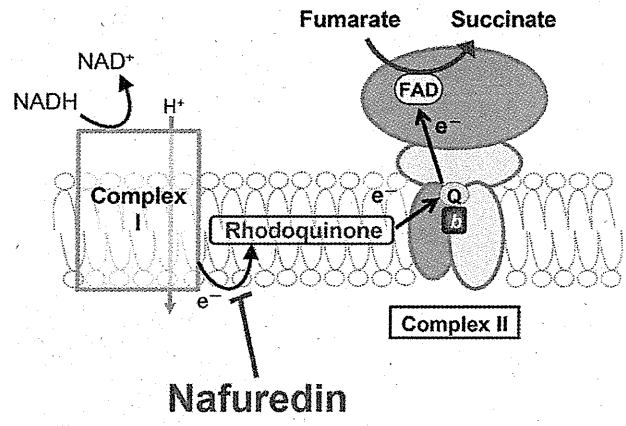

Fig. 5. NADH-fumarate reductase System of *A. suum* as a target of chemotherapy.The differences in energy metabolisms between host and helminths are an attractive therapeutic targets for helminthiasis. NADH-fumarate reductase is a part of a unique respiratory system in parasitic helminths and is the terminal step of the phospho*enol*pyruvate carboxykinase–succinate pathway, which is found in many anaerobic organisms. NADH-fumarate reductase system is a potential target for chemotherapy. Nafuredin was found to be competitive inhibitor for rhodoquinone binding site of *A. suum* complex II [1].

described in the previous section. This system is also called "fumarate respiration". The low-potential rhodoquinone transfers reducing equivalent of NADH via complex I to complex II, and finally succinate is produced by quinol fumarate reductase (QFR) activity of complex II. The merit of this system is to synthesize ATP using the coupling site of complex I even in the absence of oxygen, although its energy efficiency is low (Fig. 5).

A similar anaerobic respiration system exists in the mitochondria of many other parasites, and has also been found in bacteria. Extensive studies of bacteria, including *E. coli*, have revealed the details of this system [23,24]. In *E. coli*, there are two types of complex II, and QFR encoded by the *frd* operon is induced under anaerobic conditions. A low molecular weight mediator between complex I and complex II is menaquinone (MK; $Em' = -80$ mV), a low-potential naphthoquinone, in the *E. coli* fumarate respiration. In contrast, under aerobic conditions, SQR encoded by *sdh* operon that catalyzes oxidation of succinate is induced [25]. SQR is a dehydrogenase complex in the respiratory system as well as an enzyme in the TCA cycle, and directly connects these systems in aerobic energy metabolism.

Thus, two different enzymes (complex II) are present in *E. coli*, and the bacteria maintain homeostasis of the energy metabolism by controlling the synthesis of these enzymes in response to the environmental oxygen supply. How about the complex IIs of *A. suum*? Biochemical and molecular biological analyses showed *A. suum* also possesses two different complex IIs. However, subunit compositions and expression patterns are more complicated in the parasite complex II.

3. Complex IIs of *A. suum* mitochondria

3.1. Multiple complexes II in A. suum mitochondria

The complex II superfamily comprises succinate–quinone reductase (SQR) and quinol–fumarate reductase (QFR), which catalyze the interconversion of succinate and fumarate with quinone and quinol. SQR is a component of the aerobic respiratory chain as well as the tricarboxylic acid (TCA) cycle [26]. QFR is a component of the anaerobic respiratory chain in anaerobic and facultative anaerobic bacteria [27] and lower eukaryotes [6,28]. SQR and QFR complexes generally consist of four subunits referred to as the flavoprotein subunit (Fp), iron–sulfur subunit (Ip), cytochrome *b* large subunit (CybL), and cytochrome *b* small subunit (CybS). The Fp and Ip subunits comprise the catalytic domain of the enzyme. The Fp subunit has a FAD as a prosthetic group and contains the dicarboxylate-binding site. The Ip subunit generally contains three iron–sulfur clusters $[2Fe\text{–}2S]^{2+,1+}$, $[4Fe\text{–}4S]^{2+,1+}$, and $[3Fe\text{–}4S]^{1+,0}$. Subunits CybL and CybS, with heme *b* as the prosthetic group, form the anchor domain of the enzyme. This anchors the catalytic domain to the inner mitochondrial membrane and also serves as the quinone oxidation/reduction site [29].

Our previous study showed that *A. suum* mitochondria express stage-specific isoforms of complex II (SQR in larvae/QFR in adult) (Fig. 6). The Fp and CybS in adult complex II differ from those of infective third stage larval (L3) complex II. In contrast, there is no difference in the iron-sulfur cluster (Ip) and CybL between adult and L3 isoforms of complex II. However, recent analysis of the changes that occur in the respiratory chain of *A. suum* larvae during their migration in the host, we found that enzymatic activity, quinone content and complex II subunit composition in mitochondria of lung stage L3 (LL3) *A. suum* larvae is different from those of L3 and adult [22]. Quantitative analysis of quinone content in LL3 mitochondria showed that ubiquinone is more abundant than rhodoquinone. Interestingly, the results of two-dimensional bule-native/sodium dodecyl sulfate polyacrylamide gel electrophoresis analyses showed that LL3 mitochondria contained larval Fp (Fp^L) and adult Fp (Fp^A) at a ratio of 1:0.56, and that most LL3 CybS subunits were of the adult form ($CybS^A$). This result clearly indicates that the rearrangement of complex II begins with a change in the isoform of the anchor CybS subunit, followed by a similar change in the Fp subunit. At any event, the NADH-fumarate reductase activity of *A. suum* adult worms (~100 nmol/min/mg) are much higher than that of the mammalian host (2~5 nmol/min/mg).

3.2. ROS production from complex II

Mitochondrial respiratory chain is a significant source of cellular ROS. Impairment of the respiratory chain complexes is known to

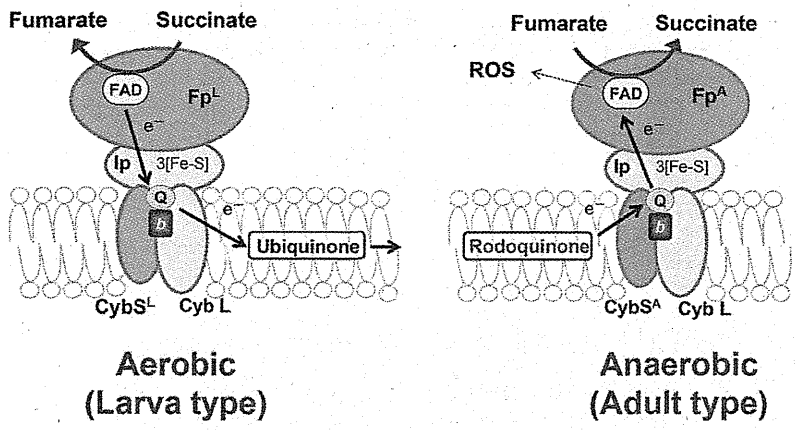

Fig. 6. Schematic representation of *A. suum* complexes II from larva type and adult type.The mitochondrial metabolic pathway of the parasitic nematode *A. suum* changes dramatically during its life cycle, to adapt to changes in the environmental oxygen concentration. *A. suum* mitochondria express stage-specific isoforms of complex II. While there is no difference in the isoforms of the Ip and cybL subunits of complex II between L3 larvae and adult A. *suum*, they have different isoforms of complex II subunits Fp (larval, Fp^L; adult, Fp^A) and cybS (larval, $cybS^L$; adult, $cybS^A$) in *A. suum* adult respiratory chain, complex II produces high amount ROS [29].

increase the cellular ROS production [30]. In general, complexes I and III are considered as the two major sites of superoxide and hydrogen peroxide production in the respiratory chain [30–33]. Interestingly, our results show that complex II is the main site of ROS production in *A. suum* adult respiratory chain [9].

Analysis of submitochondrial particles for superoxide ($O_2^{\cdot-}$) production using superoxide dismutase inhibitable acetylated cytochrome *c* reduction, and hydrogen peroxide production using catalase inhibitable amplex red oxidation, in the presence and absence of respiratory chain inhibitors, showed the contribution from both the FAD site and quinone-binding site of complex II to produce $O_2^{\cdot-}$ and H_2O_2 when succinate is oxidized under aerobic conditions. Considering the conservation of amino acid residues critical for the enzyme reaction between *A. suum* complex II and mitochondrial SQR, our results show the ROS production from more than one site in mitochondrial complex II linked with subtle differences in the amino acid sequences of the enzyme complex.

A. suum adult complex II is a good model to study the mechanism of ROS production from mitochondrial complex II, since amino acid residues conserved among the catalytic domains in mitochondrial SQR enzymes are well conserved in this enzyme and it produces high levels of ROS. Absence of complex III and IV activities in its respiratory chain is an additional advantage of this model. These studies will provide further insight into the possibility of high levels of ROS production from both the FAD site and the Q site in the complex II of *A. suum* adult worm and help to understand the role of mutations in human complex II for carcinogenesis.

3.3. Specific inhibitors of complex II

The differences between parasite and host mitochondria described in this review hold great promise as targets for chemotherapy. For example, the anti-malarial drug Atovaquone, which was recently developed, acts on the mitochondrial respiratory chain [34]. Atovaquone is effective against chloroquine-resistant strains, [35]. The specific target is thought to be complex III, and biochemical analysis has shown that it acts on the ubiquinone oxidation site in the cytochrome *b* of complex III [36,37]. Such a chemotherapeutic approach is also applicable to the helminthes. It has been proposed that the fumarate respiration is the target of such drugs as bithionol and thiabendazole [38,39], but there is no clear biochemical or pharmaceutical evidence to support this idea. However, as described in the previous section, progress in the study of the NADH-fumarate reductase pathway permits screening of new anthelmintic compound. Nafuredin, selectively inhibits helminth complex I at concentrations in the order of nanomoles [40] (Fig. 7). Kinetic analysis revealed that the inhibition by nafuredin is competitive against RQ (Fig. 5). These findings, coupled with the fact that helminth complex I uses both RQ and UQ as an electron acceptor, suggest that the structural features of the quinone reduction site of helminth complex I may differ from that of mammalian complex I. In fact, the inhibitory mechanism of quinazolines, which effectively kill the *E. multilocularis* protoscoleces, was competitive and partially competitive against RQ and UQ, respectively [41].

The most potent inhibitor of complex II, Atpenin A5, was found during the screening of inhibitors for *A. suum* complex II [42]. To our regret, IC_{50} of Atpenin A5 for bovine complex II (3.6 nM) was lower than that for *A. suum* complex II (12 nM for QFR and 32 nM for SQR). However, further screening of inhibitors showed that flutolanil, a commercially available fungicide, specifically inhibits *A. suum* SQR [43] (Fig. 7). The IC_{50} of flutolanil against *A. suum* and bovine SQR was 0.081 and 16 μM, respectively, indicating that flutolanil is a promising lead compound for anthelminthics. To enable rational drug optimization, a crystal of the *A. suum* QFR complexed with

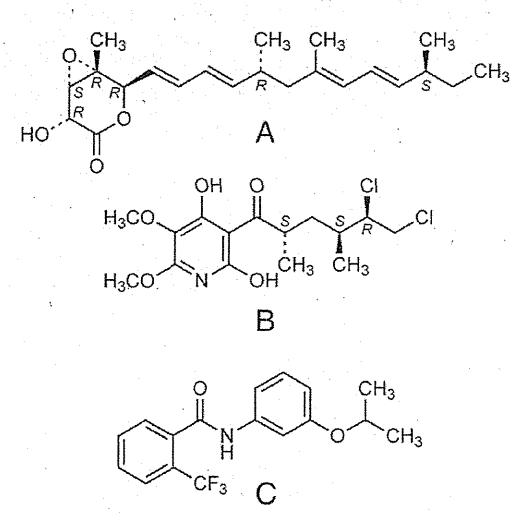

Fig. 7. Chemical structure of inhibitors of complex II.A. Nafuresin, a competitive inhibitor for the rhodoquinone binding site of *A. suum* complex II; B. Atpenin A5, a competitive inhibitor for the quinone binding site of complex II of many species; C. Fulutolanil, a competitive inhibitor for the quinone binding site of *A. siuum* complex II.

flutolanil was prepared by soaking, and X-ray structure analysis has been performed. The current structural model of the flutolanil bound form of the *A. suum* QFR (Harada, unpublished observation) indicates that flutolanil is bound to the same site as those of the quinone binding observed in complex IIs from pig heart mitochondria (pdb code 1ZOY), *E. coli* (1NEK and 1L0V) and avian (1YQ4). The site of the pig enzyme, for example, is composed of ten residues highly conserved across amino acid sequences of these complex IIs; Pro169, Trp173 and Ile218 from the Ip subunit, Ile30, Trp35, Met39, Ser42, Ile43 and Arg46 from the CybL subunit, and Tyr91 from the CybS subunit. However, three residues, Trp35, Met39 and Ile53, are replaced by Pro65, Trp69 and Gly73, respectively, in *A. suum* QFR. The structures of the *A. suum* QFR together with those of QFRs from *Wolinella succinogenes* [24] and *E. coli* [23], and SQRs from *E. coli* [44], pig heart mitochondria [45], and avian heart mitochondria [46] should help clarify the structure–function relationship of complex II and provide useful information for the structure-based design of anthelminthics.

4. Fumarate respiration of human mitochondria

4.1. Human complex II

In human, many cases of diseases caused by mutations in subunits of complex II have been reported. Mutations found in the Ip, Cyb L or Cyb S are associated with the development of pheochromocytoma and paraganglioma [47–51]. It is suggested that the causes of tumorigenesis are ROS production from mutated complex II [52,53] or accumulation of succinate as a result of SQR inhibition [11]. Accumulated succinate inhibits HIF-1α prolyl hydroxylases in the cytosol, leading to stabilization and activation of HIF-1α. Thus, succinate can increase expression of genes that facilitate angiogenesis, metastasis, and glycolysis, ultimately leading to tumor progression. On the other hand, no patient with mutation in Fp linked to tumorigenesis has been reported. There are two Fp isoforms in human, which will be discussed later, and this is probably the reason why mutations in Fp are not directly linked to tumorigenesis. Instead, mutations in Fp are linked to severe metabolic disorders resulting from decreased activity of the TCA cycle and impairment of oxidative phosphorylation, although these are rare. These autosome-recessive disorders are manifested as childhood encephalopathy, myopathy, adult optic atrophy, and Leigh syndrome [54–57]. Recently, two new proteins, SDHAF1 (succinate dehydrogenase complex assembly factor 1) and SDHAF2, were found to be the first assembly factors of complex II [53,58]. It was suggested that mutations found in SDHAF1 may result in the reduction of assembled complex II and cause infantile leukoencephalopathy [58]. SDHAF2 is suggested to be required for the incorporation of the flavin adenine dinucleotide cofactor (flavination) of SDHA (succinate dehydrogenase complex, subunit A, flavoprotein), and it is also necessary for complex II assembly and function [53]. Furthermore, the mutation found in SDHAF2 has been suggested to link to familial paraganglioma [53]

4.2. Isoforms of human complex II

In 2003, we found two isoforms of human Fp, type I and type II [59,60] (Fig. 8). These isoforms differ from each other only in two amino acid residues. Tyr 586 and Val 614 of type I Fp are replaced by Phe 586 and Ile 614 in type II Fp, respectively. Tyr 586 and Val 614 are well conserved among mammals' Fps and type II Fp is found only in human complex II (Fig. 9). Type I Fp gene has an exon–intron structure, while the structure of type II Fp gene has not been determined. The type II Fp gene is not found in the NCBI database and the location has not been clarified yet while type I Fp gene is located on chromosome 5p15 [59,60].

Complex II with type I Fp has isoelectric point (p*I*) of 6–7, whereas complex II with type II Fp shows its p*I* of 5–6. To explain the difference of p*I* values, several reports suggested the phosphorylation of amino acid residues in Fp subunit [7,61]. One of these residues, Tyr 500, is located close to Tyr 586, which is replaced by Phe in type II Fp (Fig. 10). Since the Tyr 586 Phe substitution will certainly destroy a hydrogen bond between Tyr 586 O_η and Glu 597 O_δ (3.13Å), the local structure around Tyr 586 as well as Tyr 500 phosphorylation status may be different between Fps of types I and II.

The result of biochemical analysis of complex II with each isoform, complex II with each Fp was found to have almost the same SQR specific activities. However, type II Fp has lower optimal pH than type I Fp and at optimal pH of type II Fp, K_m value for succinate of type II Fp is lower than type I Fp (Sakai unpublished data). It may be possible that different phosphorylation statuses of complex II with each isoform cause biochemical differences.

4.3. Expression of human complex II containing type II Fp

Our previous study on the expression of isoforms showed that both types were expressed in all the organs tested (liver, heart, skeletal muscle, brain and kidney) and expression of type I Fp was higher than that of type II Fp [59,60]. This tendency was also found in the cultured cells such as Fibroblast, Myoblast, Human Umbilical Vein Endothelial Cells (HUV-EC-C), colon cancer cells (HT-29) and lung cancer cells (A549). However, colorectal adenocarcinoma cells (DLD-1), breast cancer cells (MCF-7) and lymphoma cells (Raji) showed higher expression of type II than that of type I Fp. Type I Fp seems to be essential for the ordinary function of complex II because

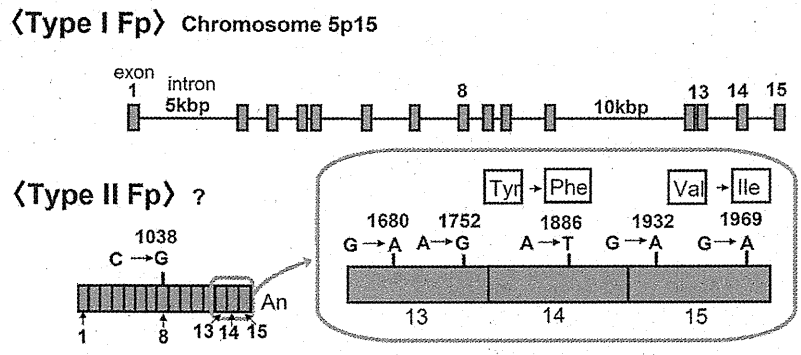

Fig. 8. Fp isoform gene structure.Type I and II Fps differ from each other in six bases in DNA sequences and in two amino acid residues in proteins. Type I Fp gene has an exon–intron structure, while type II Fp gene issuggested to be intron-less. Although type I Fp gene is located on chromosome 5p15, the type II Fp gene is not found in the NCBI database and the location has not been clarified yet [59,60].

```
Human type I Fp   578  HWRKHTLSYVDVGTGKVTLEYRPVI DKTLNEADCATVPPAI RSY
Human type II Fp  578  HWRKHTLSFVDVGTGKVTLEYRPVI DKTLNEADCATIPPAI RSY
Rat Fp            570  HWRKHTLSYVDTKTGKVTLDYRPVI DKTLNEADCATVPPAI RSY
Mouse Fp          578  HWRKHTLSYVDIKTGKVTLEYRPVI DKTLNEADCATVPPAI RSY
Bovine Fp         582  HWRKHTLSYVDIKTGKVTLEYRPVI DRTLNETDCATVPPAI GSY
                            Y586F                    V614I
```

Fig. 9. Alignment of amino acid sequences of Mammalian Fp subunits.Two amino acid residues in the red box are different in human Fp isoforms. Tyr 586 and Val 614 in type I Fp are changed to Phe 586 and Ile 614 in type II Fp, respectively. Tyr 586 and Val 614 are well conserved among mammals and no animals but humans have type II Fp [59].

all the examined tissues and many of the cultured cells showed abundant expression of type I Fp and optimum pH for this isoform is around physiological mitochondrial matrix pH (pH8.0).

Since type II Fp was expressed in some cancer cells, this isoform may play an important role in the metabolism of tumor tissue. To investigate the link between type II Fp and tumor tissue in detail, we analyzed mRNA expression ratio of Fp isoforms in several tissues including tumor tissues and cultured cells. Since some tumor marker genes are expressed in fetal tissues, we included the fetal tissues in this analysis.

As shown in Table 1, in cultured cells, all the normal cells tested showed mainly type I Fp expression as reported previously [59,60]. In tissues, expression of type I Fp was higher than that of type II Fp in all the organs tested including normal testes tissue. Interestingly, normal pancreatic tissue showed higher expression of type II Fp. In addition, several tumor tissues expressed predominantly type II Fp such as breast tumor, liver tumor, kidney tumor and cervix tumor. Among fetal tissues, brain and skeletal muscle showed higher expression of type II Fp than type I Fp.

4.4. Fumarate respiration of human cancer cells

Several observations suggested the presence of a reverse reaction of complex II, fumarate reductase (FRD), in mammalian cells, although no direct evidence of FRD activity in mammalian complex II has been available until recently [62,63]. The accumulation of succinate under hypoxic conditions has been reported, and complex II has been suggested to function as FRD in mammalian cells [64]. Metabolome analysis of the cancer cells supports this idea, because succinate, fumarate and malate were present at higher levels in cancer tissues than normal tissues [65]. FRD inhibitor pyrvinium pamoate, an anthelmintic, has also been reported to act as an anticancer compound in human cancer cells [62]. Furthermore, recent biochemical studies showed fumarate respiration in human mitochondria clearly [7,8]. Mitochondria isolated from DLD-1 cells showed FRD activity with 3 nmol/min/mg protein, although this number is quite lower than that of the *A. suum* mitochondria (200 nmol/min/mg). Interestingly, the cancer cells had higher FRD/SQR ratio than the normal cells. For example, FRD/SQR ratio in Panc-1 cells is 0.066 ± 0.010, while that in Human Dermal Fibroblast cells is 0.011 ± 0.002. In addition, FRD/SQR ratio increased when the cancer cells were cultured under hypoxic and glucose limited condition [7]. Effect of a treatment by phosphatase and protein kinase on the direction of enzyme activity of human complex II suggests the changes from SQR to QFR by phosphorylation of Fp.

Different from *A. suum*, which has at least two distinct complex IIs as mentioned previously, only one gene is found for each subunit of human complex II except Fp. In this connection, it is of interest to speculate that complex II with type II Fp has higher QFR activity and plays an important role in fumarate respiration in human mitochondria as terminal oxidase of the system. Further biochemical study on

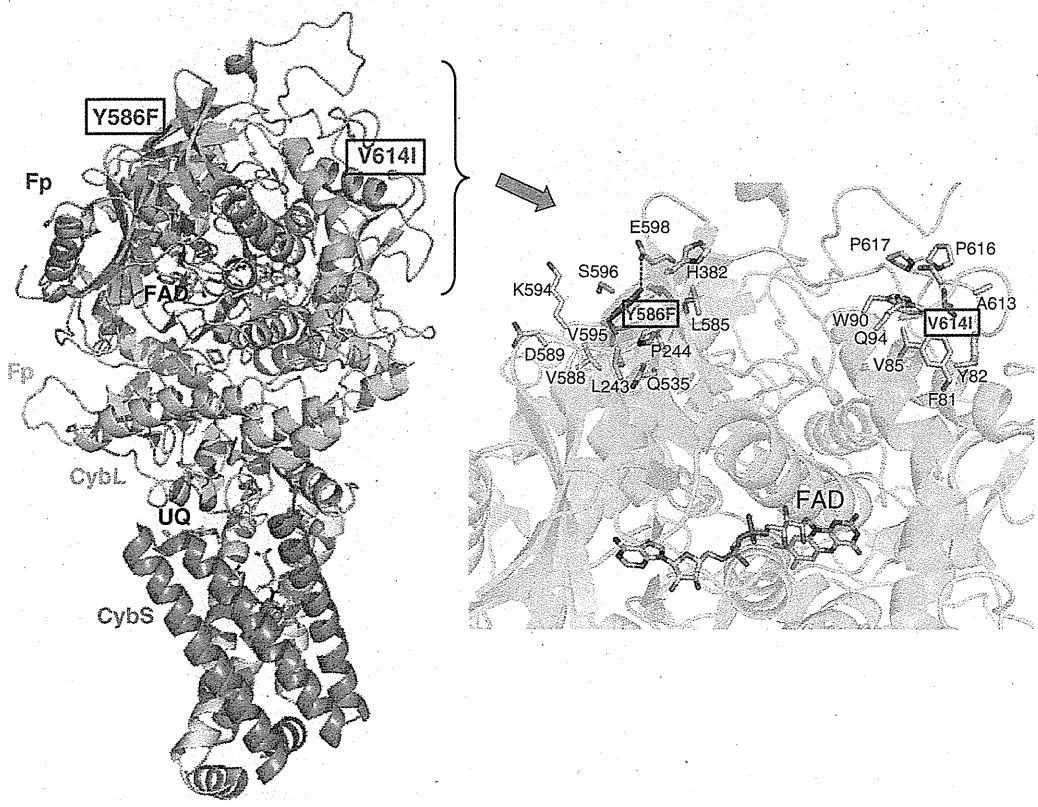

Fig. 10. Positions of Tyr 586 and Val 614 in the structure of porcine complex II.Two amino acid residues different in human isoforms, Y586F and V614I, shown in the cartoon representation of the porcine complex II structure (left) and the close-up view of the region including Y586F and V614I (right). V614I is surrounded mainly by hydrophobic residues, whereas Y586F by both hydrophilic and hydrophobic residues. Y586 and E598 are in the hydrogen bond distance (3.15 Å) to each other. UQ shows ubiquinone. The numbers of amino acid residues in the box represent the human amino acid sequences and the others are the porcine amino acid sequences.

Table 1
mRNA expression of Fp isoforms in human cultured cells and tissues.

The expression ratio of the two Fp isoforms was analyzed by RT-PCR-RFLP (restriction fragment length polymorphism with AvaII). Total RNAs were obtained from NIPPON GENE (Japan) for normal liver, heart, skeletal muscle, brain, kidney and breast tumor, colon tumor, stomach tumor and uterus tumor. Wako (Japan) for normal pancreas and fetal tissues. Invitrogen (USA) for normal testes and breast tumor, liver tumor, kidney tumor, colon tumor, pancreas tumor, cervix tumor, ovary tumor, prostate tumor. Cells; Fibroblast and Myoblast: kind gift from Dr. Yu-ichi Goto (National Institute of Neuroscience, Japan) A549, DLD-1 and MCF-7: kind gift from Mr. Yasuyuki Yamazaki (Taiho pharma ceutical, Japan) Panc-1: kind gift from Dr. Yasuhiro Esumi (National Cancer Institute, Japan) Raji: kind gift from Dr. Kazurou Shiomi (Kitasato university, Japan) HT-29, HU-VEC-C, MDA-M-231, BT-20 and T-47D: ATCC (USA). Pancreatic epithelial and stromal cells: DS pharma (Japan).

		Race	Gender	Age	I (%)/II (%)
Tissue (normal)	Liver*	Caucasoid	Female	15	70/30
	Heart*	Caucasoid	Pool of 7 donors		61/39
	Skeletal muscle*	—	Male	23	80/20
	Brain*	Caucasoid	Male	50	84/16
	Kidney*	Caucasoid	Pool of 8 donors		62/38
	Pancreas	—	Male	44	30/70
	Testes	Caucasoid	Male	19	100/0
Cell (normal)	Fibroblast*	Mongoloid	—	—	94/6
	Myoblast*	Mongoloid	—	—	87/13
	HUV-EC-C*	—	—	—	88/12
	Pancreatic epithelial	—	—	—	100/0
	Pancreatic stromal	—	—	—	100/0
Tissue (fetal)	Brain	—	Female	22 weeks	100/0
	Brain	—	Male	41 weeks	38/62
	Skeletal muscle	—	Male	22 weeks	0/100
	Skeletal muscle	—	Female	19 weeks	100/0
Tissue (cancer)	Breast	—	Female	55	100/0
	Breast	Mongoloid	Female	Pool of 6 donors	0/100
	Liver	Caucasoid	Male	60	0/100
	Kidney	Caucasioid	Female	54	23/77
	Colon	Caucasoid	Male	75	100/0
	Colon	—	—	—	100/0
	Pancreas	Mongoloid	Male	32	100/0
	Stomach	—	—	—	100/0
	Uterus	—	Female	—	100/0
	Cervix	Caucasoid	Female	59	23/77
	Ovary	Caucasoid	Female	32	100/0
	Prostate	—	Male	—	100/0
Cell (cancer)	HT29*	Caucasoid	Female	44	92/8
	A549*	Caucasoid	Male	58	96/4
	DLD-1*	—	Male	—	25/75
	MCF-7*	Caucasoid	Female	69	23/77
	Raji*	Neglod	Male	11	17/83
	Panc-1	Caucasoid	Male	56	12/88
	MDA-M-231	Caucasoid	Female	51	100/0
	BT-20	Caucasoid	Female	78	78/22
	T-47D	Caucasoid	Female	54	53/47

* Tomitsuka, et al. [59,60].

the difference between type I and type II Fp will bring final conclusion on this attractive idea.

5. Conclusions

The recent findings described in this review indicate that the respiratory chain plays an important role in responses to changes in the amount of oxygen in the environment. Complex II functions as a fumarate reductase during adaptation to a hypoxic condition to ensure the maintenance of oxygen homeostasis. In this connection, the reports indicating that complex II functions as an oxygen sensor are of great interest [63].

In addition, direct evidence of fumarate respiration in human mitochondria are quite important in the study of energy metabolism in hypoxic condition including cancer cells. Differences in energy metabolism between hosts and parasites and/or cancer cells are attractive therapeutic targets.

Acknowledgements

This work was supported in part by Creative Scientific Research Grant 18GS0314 (to KK), Grant-in-aid for Scientific Research on Priority Areas 18073004 (to KK) from the Japanese Society for the Promotion of Science, and Targeted Proteins Research Program (to KK) from the Japanese Ministry of Education, Science, Culture, Sports and Technology (MEXT).

References

[1] K. Kita, K. Shiomi, S. Ōmura, Parasitology in Japan: advances in drug discovery and biochemical studies, Trends Parasitol. 23 (2007) 223–229.
[2] A. Kroger, V. Geisler, E. Lemma, F. Theis, R. Lenger, Bacterial fumarate respiration, Arch. Microbiol. 158 (1992) 311–314.
[3] T. Kuramochi, H. Hirawake, S. Kojima, S. Takamiya, R. Furushima, T. Aoki, R. Komuniecki, K. Kita, Sequence comparison between the flavoprotein subunit of the fumarate reductase (complex II) of the anaerobic parasitic nematode, *Ascaris suum* and the succinate dehydrogenase of theaerobic, free-living nematode, *Caenorhabditis elegans*, Mol. Biochem. Parasitol. 68 (1994) 177–187.
[4] F. Saruta, H. Hirawake, S. Takamiya, Y.-C. Ma, T. Aoki, K. Sekimizu, S. Kojima, K. Kita, Cloning of a cDNA encoding the small subunit of cytochrome b_{558} (cybS) of mitochondrial fumarate reductase (complex II) from adult *Ascaris suum*, Biochim. Biophys. Acta 1276 (1996) 1–5.
[5] H. Amino, H. Wang, H. Hirawake, F. Saruta, D. Mizuchi, R. Mineki, N. Shindo, K. Murayama, S. Takamiya, T. Aoki, S. Kojima, K. Kita, Stage-specific isoforms of *Ascaris suum* complex II: the fumarate reductase of the parasitic adult and the succinate dehydrogenase of free-living larvae share a common iron-sulfur subunit, Mol. Biochem. Parasitol. 106 (2000) 63–76.
[6] K. Kita, S. Takamiya, Electron-transfer complexes in *Ascaris* mitochondria, Adv. Parasitol. 51 (2002) 95–131.
[7] E. Tomitsuka, K. Kita, H. Esumi, Regulation of succinate–ubiquinone reductase and fumarate reductase activities in human complex II by phosphorylation of its flavoprotein subunit, Proc. Jpn. Acad. Ser. B Phys. Biol. Sci. 85 (2009) 258–265.
[8] E. Tomitsuka, K. Kita, H. Esumi, The NADH-fumarate reductase system, a novel mitochondrial energy metabolism, is a new target for anticancer therapy in tumor microenvironments, Ann. N. Y. Acad. Sci. 201 (2011) 44–49.
[9] M.P. Paranagama, K. Sakamoto, H. Amino, M. Awano, H. Miyoshi, K. Kita, Contribution of the FAD and quinone binding sites to the production of reactive oxygen species from *Ascaris suum* mitochondrial complex II, Mitochondrion 10 (2010) 158–165.
[10] R.D. Guzy, B. Sharma, E. Bell, N.S. Chandel, P.T. Schumacker, Loss of the SdhB, but Not the SdhA, subunit of complex II triggers reactive oxygen species-dependent hypoxia-inducible factor activation and tumorigenesis, Mol. Cell. Biol. 28 (2008) 718–731.
[11] M.A. Selak, S.M. MacKenzie, H. Boulahbel, D.G. Watson, K.D. Mansfield, Y. Pan, M.C. Simon, C.B. Thompson, E. Gottlieb, Succinate links TCA cycle dysfunction to oncogenesis by inhibiting HIF-alpha prolyl hydroxylase, Cancer Cell 7 (2005) 77–85.
[12] R. Komuniecki, B.G. Harris, J. Marr, M. Mueller, Biochemistry and Molecular Biology of Parasites, Academic Press, London, 1995, pp. 49–66.
[13] A.G.M. Tielens, J. Van Hellemond, The electron transport chain in anaerobically functioning eukaryotes, Biochim. Biophys. Acta 1365 (1998) 71–78.
[14] K. Kita, H. Hirawake, S. Takamiya, Cytochromes in the respiratory chain of helminth mitochondria, Int. J. Parasitol. 27 (1997) 617–630.
[15] J. Matsumoto, K. Sakamoto, N. Shinjyo, Y. Kido, N. Yamamoto, K. Yagi, H. Miyoshi, N. Nonaka, K. Katakura, K. Kita, Y. Oku, Anaerobic NADH-fumarate reductase system is predominant in the respiratory chain of *Echinococcus multilocularis*, providing a novel target for the chemotherapy of alveolar echinococcosis, Antimicrob. Agents Chemother. 52 (2008) 164–170.
[16] P. Kohler, R. Bachmann, Mechanisms of respiration and phosphorylation in *Ascaris* muscle mitochondria, Mol. Biochem. Parasitol. 1 (1980) 75–90.
[17] H. Oya, K. Kita, in: E. Bennet, C. Behm, C. Bryant (Eds.), Comparative Biochemistry of Parasitic Helminths, Chapman and Hall, London, 1988, pp. 35–53.
[18] S. Takamiya, R. Furushima, R.H. Oya, Electron transfer complexes of *Ascaris suum* muscle mitochondria: I. Characterization of NADH-cytochrome *c* reductase (complex I–III), with special reference to cytochrome localization, Mol. Biochem. Parasitol. 13 (1984) 121–134.
[19] S. Takamiya, K. Kita, H. Wang, P.P. Weinstein, A. Hiraishi, H. Oya, T. Aoki Developmental, Changes in the respiratory chain of *Ascaris* mitochondria, Biochim. Biophys. Acta 1141 (1993) 65–74.
[20] S.T. Cole, C. Condon, B.D. Lemire, J.H. Weiner, Molecular biology, biochemistry and bioenergetics of fumarate reductase, a complex membrane-bound iron–sulfur flavoenzyme of *Escherichia coli*, Biochim. Biophys. Acta 811 (1985) 381–403.
[21] A. Hiraishi, Fumarate reduction systems in members of the family *Rhodospirillaceae* with different quinone types, Arch. Microbiol. 150 (1988) 56–60.
[22] F. Iwata, N. Shinjyo, H. Amino, K. Sakamoto, M.K. Islam, N. Tsuji, K. Kita, Change of subunit composition of mitochondrial complex II (succinate–ubiquinone reductase/quinol–fumarate reductase) in *Ascaris suum* during the migration in the experimental host, Parasitol. Int. 57 (2008) 54–61.

[23] T.M. Iverson, C. Luna-Chavez, G. Cecchini, D.C. Rees, Structure of the *Escherichia coli* fumarate reductase respiratory complex, Science 284 (1999) 1961–1966.
[24] C.R. Lancaster, A. Kröger, M. Auer, H. Michel, Structure of fumarate reductase from *Wolinella succinogenes* at 2.2 A resolution, Nature 402 (1999) 377–385.
[25] K. Kita, C. Vibat, S. Meinhardt, J. Guest, R. Gennis, One-step purification from *Escherichia coli* of complex II (succinate: ubiquinone oxidoreductase) associated with succinate-reducible cytochrome b_{556}, J. Biol. Chem. 264 (1989) 2672–2677.
[26] G. Cecchini, I. Schroder, R.P. Gunsalus, E. Maklashina, Succinate dehydrogenase and fumarate reductase from *Escherichia coli*, Biochim. Biophys. Acta 1553 (2002) 140–157.
[27] C.R.D. Lancaster, Structure and function of succinate: quinone oxidoreductases and the role of quinol: fumarate reductases in fumarate respiration, in: D. Zannoni (Ed.), Respiration in Archaea and Bacteria: Diversity of Prokaryotic Electron Transport Carriers, Kluwer Academic Publishers, The Netherlands, 2004, pp. 57–85.
[28] J.J. Van Hellmond, A. van der Klei, S.W.H. van Weelden, A.G.M. Tielens, Biochemical and evolutionary aspects of anaerobically functioning bacteria, Philos. Trans. R. Soc. B 358 (2003) 205–215.
[29] K. Kita, H. Hirawake, H. Miyadera, H. Amino, S. Takeo, Role of complex II in anaerobic respiration of the parasite mitochondria from *Ascaris suum* and *Plasmodium falciparum*, Biochim. Biophys. Acta 1553 (2002) 123–139.
[30] H.P. Indo, M. Davidson, H.C. Yen, S. Suenaga, K. Tomita, T. Nishii, M. Higuchi, Y. Koga, T. Ozawa, H.J. Majima, Evidence of ROS generation by mitochondria in cells with impaired electron transport chain and mitochondrial DNA damage, Mitochondrion 7 (2007) 106–118.
[31] P. Jezek, L. Hlavata, Mitochondria in homeostasis of reactive oxygen species in cell, tissues, and organism, Int. J. Biochem. Cell Biol. 37 (2005) 2478–2503.
[32] M.P. Murphy, How mitochondria produce reactive oxygen species, Biochem. J. 417 (2009) 1–13.
[33] J. St-Pierre, J.A. Buckingham, S.J. Roebuck, M.D. Brand, Topology of superoxide production from different sites in the mitochondrial electron transport chain, J. Biol. Chem. 277 (2002) 44784–44790.
[34] I.K. Srivastava, H. Rottenberg, A.B. Vaidya, Atovaquone, a broad spectrum antiparasitic drug, collapses mitochondrial membrane potential in a malarial parasite, J. Biol. Chem. 272 (1997) 3961–3966.
[35] S. Looareesuwan, C. Viravan, H.K. Webster, D.E. Kyle, D.B. Hutchinson, C.J. Canfield, Clinical studies of atovaquone, alone or in combination with other antimalarial drugs, for treatment of acute uncomplicated malaria in Thailand, Am. J. Trop. Med. Hyg. 54 (1996) 62–66.
[36] D. Syafruddin, J.E. Siregar, S. Marzuki, Mutations in the cytochrome *b* gene of *Plasmodium berghei* conferring resistance to atovaquone, Mol. Biochem. Parasitol. 104 (1999) 185–194.
[37] I.K. Srivastava, J.M. Morrisey, E. Darrouzet, F. Daldal, A.B. Vaidya, Resistance mutations reveal the atovaquone-binding domain of cytochrome *b* in malaria parasites, Mol. Microbiol. 33 (1999) 704–711.
[38] P. Kohler, R. Bachmann, The effects of the antiparasitic drugs levamisole, thiabendazole, praziquantel, and chloroquine on mitochondrial electron transport in muscle tissue from *Ascaris suum*, Mol. Biochem. Parasitol. 14 (1978) 155–163.
[39] A. Armson, W.B. Grubb, A.H.W. Mendis, The effect of electron transport (ET) inhibitors and thiabendazole on the fumarate reductase (FR) and succinate dehydrogenase (SDH) of *Strongyloides ratti* infective (L3) larvae, Int. J. Parasitol. 25 (1995) 261–263.
[40] S. Omura, H. Miyadera, H. Ui, K. Shiomi, Y. Yamaguchi, R. Masuma, T. Nagamitsu, D. Takano, T. Sunazuka, A. Harder, H. Kölbl, M. Namikoshi, H. Miyoshi, K. Sakamoto, K. Kita, An anthelmintic compound, nafuredin, shows selective inhibition of complex I in helminth mitochondria, Proc. Natl. Acad. Sci. U. S. A. 98 (2001) 60–62.
[41] T. Yamashita, T. Ino, H. Miyoshi, K. Sakamoto, A. Osanai, E. Nakamaru-Ogiso, K. Kita, Rhodoquinone reaction site of mitochondrial complex I, in parasitic helminth, *Ascaris suum*, Biochim. Biophys. Acta 1608 (2004) 97–103.
[42] H. Miyadera, K. Shiomi, H. Ui, Y. Yamaguchi, R. Masuma, H. Tomoda, H. Miyoshi, A. Osanai, K. Kita, S. Omura, Atpenins, potent and specific inhibitors of mitochondrial complex II (succinate-ubiquinone oxidoreductase), Proc. Natl. Acad. Sci. U. S. A. 100 (2003) 473–477.
[43] A. Osanai, S. Harada, K. Sakamoto, H. Shimizu, D.K. Inaoka, K. Kita, Crystallization of mitochondrial rhodoquinol–fumarate reductase from the parasitic nematode *Ascaris suum* with the specific inhibitor flutolanil, Acta Crystallogr. Sect. F Struct. Biol. Cryst. Commun. 65 (2009) 941–954.
[44] V. Yankovskaya, R. Horsefield, S. Törnroth, C. Luna-Chavez, H. Miyoshi, C. Léger, B. Byrne, G. Cecchini, S. Iwata, Architecture of succinate dehydrogenase and reactive oxygen species generation, Science 299 (2003) 700–704.
[45] F. Sun, X. Huo, Y. Zhai, A. Wang, J. Xu, D. Su, M. Bartlam, Z. Rao, Crystal structure of mitochondrial respiratory membrane protein complex II, Cell 121 (2005) 1043–1057.
[46] L.S. Huang, G. Sun, D. Cobessi, A.C. Wang, J.T. Shen, E.Y. Tung, V.E. Anderson, E.A. Berry, 3-nitropropionic acid is a suicide inhibitor of mitochondrial respiration that, upon oxidation by complex II, forms a covalent adduct with a catalytic base arginine in the active site of the enzyme, J. Biol. Chem. 281 (2006) 5965–5972.
[47] J.P. Bayley, P. Devilee, E.M.P. Taschner, The SDH mutation database: an online resource for succinate dehydrogenase sequence variants involved in pheochromocytoma, paraganglioma and mitochondrial complex II deficiency, BMC Med. Genet. 6 (2005) 39.
[48] B.E. Baysal, On the association of succinate dehydrogenase mutations with hereditary paraganglioma, Trends Endocrinol. Metab. 14 (2003) 453–459.
[49] C. Eng, M. Kiuru, M.J. Fernandez, L.A. Aaltonen, A role for hypoxic mitochondrial enzymes in inherited neoplasia and beyond, Nat. Rev. Cancer 3 (2003) 193–202.
[50] P.J. Pollard, N.C. Wortham, I.P. Tomlinson, The TCA cycle and tumorigenesis: the examples of fumarate hydratase and succinate dehydrogenase, Ann. Med. 35 (2003) 632–639.
[51] P. Rustin, A. Rotig, Inborn errors of complex II–unusual human mitochondrial diseases, Biochim. Biophys. Acta 1553 (2002) 117–122.
[52] N. Ishii, T. Ishii, P.S. Hartman, The role of the electron transport SDHC gene on lifespan and cancer, Mitochondrion 7 (2007) 24–38.
[53] H.X. Hao, O. Khalimonchuk, M. Schraders, N. Dephoure, J.P. Bayley, H. Kunst, P. Devilee, C.W. Cremers, J.D. Schiffman, B.G. Bentz, S.P. Gygi, D.R. Winge, H. Kremer, J. Rutter, SDH5, a gene required for flavination of succinate dehydrogenase, is mutated in paraganglioma, Science 325 (2009) 1139–1142.
[54] M.A. Birch-Machin, R.W. Taylor, B. Cochran, B.A. Ackrell, D.M. Turnbull, Late-onset optic atrophy, ataxia, and myopathy associated with a mutation of a complex II gene, Ann. Neurol. 48 (2000) 330–335.
[55] T. Bourgeron, P. Rustin, D. Chretien, M. Birch-Machin, M. Bourgeois, E. Viegas-Pequignot, A. Munnich, A. Rotig, Mutation of a nuclear succinate dehydrogenase gene results in mitochondrial respiratory chain deficiency, Nat. Genet. 11 (1995) 144–149.
[56] B. Parfait, D. Chretien, A. Rötig, C. Marsac, A. Munnich, P. Rustin, Compound heterozygous mutations in the flavoprotein gene of the respiratory chain complex II in a patient with Leigh syndrome, Hum. Genet. 106 (2000) 236–243.
[57] R. Van Coster, S. Seneca, J. Smet, R. Van Hecke, E. Gerlo, B. Devreese, J. Van Beeumen, J.G. Leroy, L. De Meirleir, W. Lissens, Homozygous Gly555Glu mutation in the nuclear-encoded 70 kDa flavoprotein gene causes instability of the respiratory chain complex II, Am. J. Med. Genet. A 120 (2003) 13–18.
[58] D. Ghezzi, P. Goffrini, G. Uziel, R. Horvath, T. Klopstock, H. Lochmüller, P. D'Adamo, P. Gasparini, T.M. Strom, H. Prokisch, F. Invernizzi, I. Ferrero, M. Zeviani, SDHAF1, encoding a LYR complex-II specific assembly factor, is mutated in SDH-defective infantile leukoencephalopathy, Nat. Genet. 41 (2009) 654–656.
[59] E. Tomitsuka, H. Hirawake, Y. Goto, M. Taniwaki, S. Harada, K. Kita, Direct evidence for two distinct forms of the flavoprotein subunit of human mitochondrial complex II (succinate–ubiquinone reductase), J. Biochem. 134 (2003) 191–195.
[60] E. Tomitsuka, Y. Goto, M. Taniwaki, K. Kita, Direct evidence for expression of type II flavoprotein subunit in human complex II (succinate–ubiquinone reductase), Biochem. Biophys. Res. Commun. 311 (2003) 74–79.
[61] M. Salvi, N. Morrice, A. Brunati, A. Toninello, Identification of the flavoprotein of succinate dehydrogenase and aconitase as in vitro mitochondrial substrates of Fgr tyrosine kinase, FEBS Lett. 581 (2007) 5579–5585.
[62] H. Esumi, J. Lu, Y. Kurashima, T. Hanaoka, Antitumor activity of pyrvinium pamoate, 6-(dimethylamino)-2-[2-(2,5-dimethyl-1-phenyl-1H-pyrrol-3-yl)ethenyl]-1-me thyl-quinolinium pamoate salt, showing preferential cytotoxicity during glucose starvation, Cancer Sci. 95 (2004) 685–690.
[63] B.E. Baysal, R.E. Ferrell, J.E. Willett-Brozick, E.C. Lawrence, D. Myssiorek, A. Bosch, A. van der Mey, P.E. Taschner, W.S. Rubinstein, E.N. Myers, C.W. Richard, C.J. Cornelisse, P. Devilee, B. Devlin, Mutations in SDHD, a mitochondrial complex II gene, in hereditary paraganglioma, Science 287 (2000) 848–851.
[64] J.M. Weinberg, M.A. Venkatachalam, N.F. Roeser, I. Nissim, Mitochondrial dysfunction during hypoxia/reoxygenation and its correction by anaerobic metabolism of citric acid cycle intermediates, Proc. Natl. Acad. Sci. U. S. A. 97 (2000) 2826–2831.
[65] A. Hirayama, K. Kami, M. Sugimoto, M. Sugawara, N. Toki, H. Onozuka, T. Kinoshita, N. Saito, A. Ochiai, M. Tomita, H. Esumi, T. Soga, Quantitative metabolome profiling of colon and stomach cancer microenvironment by capillary electrophoresis time-of-flight mass spectrometry, Cancer Res. 69 (2009) 4918–4925.

J. Biochem. 2012;151(6):589–592 doi:10.1093/jb/mvs051

JB THE JOURNAL OF BIOCHEMISTRY

Rapid communication

Crystal structure of mitochondrial quinol–fumarate reductase from the parasitic nematode *Ascaris suum*

Received April 18, 2012; accepted May 1, 2012; published online May 9, 2012

Hironari Shimizu[1], Arihiro Osanai[1], Kimitoshi Sakamoto[1], Daniel Ken Inaoka[1], Tomoo Shiba[2], Shigeharu Harada[2,*] and Kiyoshi Kita[1,†]

[1]Department of Biomedical Chemistry, Graduate School of Medicine, University of Tokyo, 7-3-1 Hongo, Bunkyo-ku, Tokyo 113-0033; and [2]Department of Applied Biology, Graduate School of Science and Technology, Kyoto Institute of Technology, Sakyo-Ku, Kyoto 606-8585, Japan

*Shigeharu Harada, Department of Applied Biology, Graduate School of Science and Technology, Kyoto Institute of Technology, Sakyo-ku, Kyoto 606-8585, Japan. Tel: +81-75-724-7541; Fax: +81-75-724-7541, email: harada@kit.ac.jp

†Kiyoshi Kita, Department of Biomedical Chemistry, Graduate School of Medicine, University of Tokyo, 7-3-1 Hongo, Bunkyo-ku, Tokyo 113-0033, Japan. Tel: +81-3-5841-3526, Fax: +81-3-5841-3444, email: kitak@m.u-tokyo.ac.jp

In the anaerobic respiratory chain of the parasitic nematode *Ascaris suum*, complex II couples the reduction of fumarate to the oxidation of rhodoquinol, a reverse reaction catalyzed by mammalian complex II. In this study, the first structure of anaerobic complex II of mitochondria was determined. The structure, composed of four subunits and five co-factors, is similar to that of aerobic complex II, except for an extra peptide found in the smallest anchor subunit of the *A. suum* enzyme. We discuss herein the structure–function relationship of the enzyme and the critical role of the low redox potential of rhodoquinol in the fumarate reduction of *A. suum* complex II.

Keywords: *Ascaris suum*/crystal structure/mitochondrial respiratory complex II/rhodoquinol–fumarate reductase (QFR)/reaction mechanism.

Abbreviations: $C_{10}M$, *n*-decyl-β-D-maltoside; $C_{12}M$, *n*-dodecyl-β-D-maltoside; C_nE_m, *n*-alkyl ethylene glycol monoether; CybL, cytochrome *b* large subunit of complex II; CybS, cytochrome *b* small subunit of complex II; FAD, flavin adenine dinucleotide; Fp, flavoprotein subunit; Ip, iron–sulphur subunit; NADH, nicotinamide adenine dinucleotide; PEG, polyethyleneglycol; QFR, quinol–fumarate reductase; RQ, rhodoquinone; RQH_2, rhodoquinol; SML, sucrose monolaurate; SQR, succinate–ubiquinone reductase.

The anaerobic respiratory chain, known as the NADH-fumarate reductase (NADH-FRD) system, plays an essential role in the anaerobic energy metabolism of adult *Ascaris suum*, a parasite that inhabits the small intestine, an environment with low oxygen tension (pO_2 of ~4 mmHg). The NADH-FRD system comprises two membrane proteins, complexes I and II, embedded in the mitochondrial inner membrane. Complex I (NADH–rhodoquinone reductase) reduces rhodoquinone (RQ) to rhodoquinol (RQH_2) using the reducing equivalent of NADH, and complex II, which functions as a RQH_2–fumarate reductase (QFR), couples the reduction of fumarate to succinate to the oxidation of RQH_2 to RQ, a reverse reaction catalysed by mammalian complex II (succinate–ubiquinone reductase, SQR) of the aerobic respiratory chain. The anaerobic NADH-fumarate reductase system is found not only in *A. suum* but also in bacteria and many other parasites, and is thus a promising target for chemotherapy (*1-3*).

Although no structure is currently available for eukaryotic QFR-type complex II, structures of SQR-type complex II from porcine (*4*), avian (*5*) and *Escherichia coli* (*6*), as well as those of QFR-type from *E. coli* (*7*) and *Wolinella succinogenes* (*8*), have been determined. Their structures are similar to each other and are generally composed of four polypeptides, the largest flavoprotein subunit (Fp, 70 kDa), an iron–sulphur cluster subunit (Ip, 30 kDa), and cytochrome *b* large (CybL, 15 kDa), and small (CybS, 13 kDa) subunits. In this study, the first X-ray structural analysis of a eukaryotic QFR-type complex II was performed for *A. suum* adult complex II (*A. suum* QFR) in order to clarify the factors responsible for its QFR activity and the mechanisms of RQH_2 oxidation coupled to fumarate reduction.

Ascaris suum QFR was extracted and purified from adult *A. suum* muscle mitochondria and crystallized according to the method described by Osanai *et al.* (*9*). In brief, ~4 kg of *A. suum* obtained from a local slaughterhouse was minced and suspended in Chappell-Perry medium (100 mM KCl, 50 mM Tris–HCl pH 7.4, 5 mM magnesium sulphate, 1 mM ATP, 1 mM EDTA). The fraction containing mitochondria was separated by differential centrifugation, and *A. suum* QFR was then solubilized using 1.0% (w/v) sucrose monolaurate (SML; Dojindo). After purification with anion-exchange column chromatography, SML was exchanged with a mixture of octaethylene glycol monododecyl ether ($C_{12}E_8$) and dodecyl maltoside ($C_{12}M$) by repeated PEG3350 precipitation and dissolution in a buffer containing 0.6% (w/v) $C_{12}E_8$, 0.4% (w/v) $C_{12}M$, 200 mM NaCl, 10 mM Tris–HCl pH 7.5 and 1 mM sodium malonate. Crystallization was performed by the dialysis method using a reservoir solution containing 15% (w/v) PEG3350, 100 mM Tris–HCl pH 8.4, 200 mM NaCl,

1 mM sodium malonate, 0.06% (w/v) $C_{12}E_8$ and 0.04% (w/v) $C_{12}M$. Reddish crystals grew to 100–200 μm in 2–3 days. Crystals of *A. suum* QFR in complex with fumarate were prepared by soaking crystals in the reservoir solution supplemented with 1 mM of sodium fumarate instead of sodium malonate.

X-ray diffraction experiments were performed under a N_2 gas stream (100 K) at SPring-8 beam line BL44XU (Bruker DIP-6040 detector) and at Photon Factory beam line NW12 (ADSC315 CCD detector). Data were processed and scaled using *HKL2000* (*10*). The initial structural model of *A. suum* QFR was solved by molecular replacement using the structure of porcine complex II (pdb code: 1ZOY) as a search model. *Molrep* (*11*) was used for molecular replacement. The refinement of the structure and model building were performed using *Refmac5* (*12*) and *Coot* (*13*), respectively. Data processing and refinement statistics are shown in Supplementary Table SI. All figures were generated using *PyMOL* (*14*). The coordinates have been deposited in the Protein Data Bank under ID codes 3VR8 and 3VRB for the malonate and fumarate bound forms, respectively.

The X-ray structure of *A. suum* QFR (Fig. 1A and B) is composed of Fp, Ip, CybL and CybS subunits, with two molecules in the asymmetric unit (chains A–D and E–H, respectively). As there are no significant differences between the overall protein structures of 3VR8 and 3VRB, we will focus on chains A–D of the malonate-bound form to describe the protein structure as a whole. Fp (chain A) and Ip (chain B) are hydrophilic, whereas CybL (chain C) and CybS (chain D) are hydrophobic membrane-integrated subunits. Fp comprises four domains: a FAD binding domain (residues A33–A279 and A384–A465), a capping domain (A279–A384), a helical domain (A465–A580) and a C-terminal domain (A580–A645). A FAD prosthetic group is held in the FAD binding domain by a covalent bond to His A79 and by hydrogen bonds with highly conserved residues (Ala A49, Thr A71, Lys A72, Met A73, Ser A78, Thr A80, Gln A84, Gly A85, Gly A86, Ala A201, Asp A255, Glu A421, Arg A432, Ser A437, Leu A438) across amino acid sequences of complex IIs from various species. Ip contains an N-terminal plant ferredoxin-like domain (residues B33–B130) and a C-terminal bacterial ferredoxin-like domain (B130–B281). Of the three iron–sulphur centres bound to Ip, [2Fe–2S] is coordinated by four cysteine residues (B89, B94, B97 and B109) and located in the N-terminal domain, whereas [4Fe–4S] and [3Fe–4S] that are coordinated by four (B182, B185, B188 and B249) and three (B192, B239 and B245) cysteine residues, respectively, are bound to the C-terminal domain. These iron–sulphur centres are also surrounded with highly conserved hydrophobic amino acid residues (Fig. 1C). The structures of Fp and Ip are similar to those of complex IIs with known structures, such as *E. coli* SQR (*6*), *E. coli* QFR (*7*), *W. succinogens* QFR (*8*), porcine SQR (*4*) and avian SQR (*5*).

In contrast to Fp and Ip, the hydrophobic membrane-spanning part shows diversity among species. In *W. succinogens* QFR, it consists of a single polypeptide chain and two haem *b* prosthetic groups, whereas *A. suum* QFR, like *E. coli* SQR, porcine SQR and avian SQR, holds two polypeptide chains (CybL and CybS) and one haem *b*. Both CybL and CybS consist of three membrane-spanning α-helices

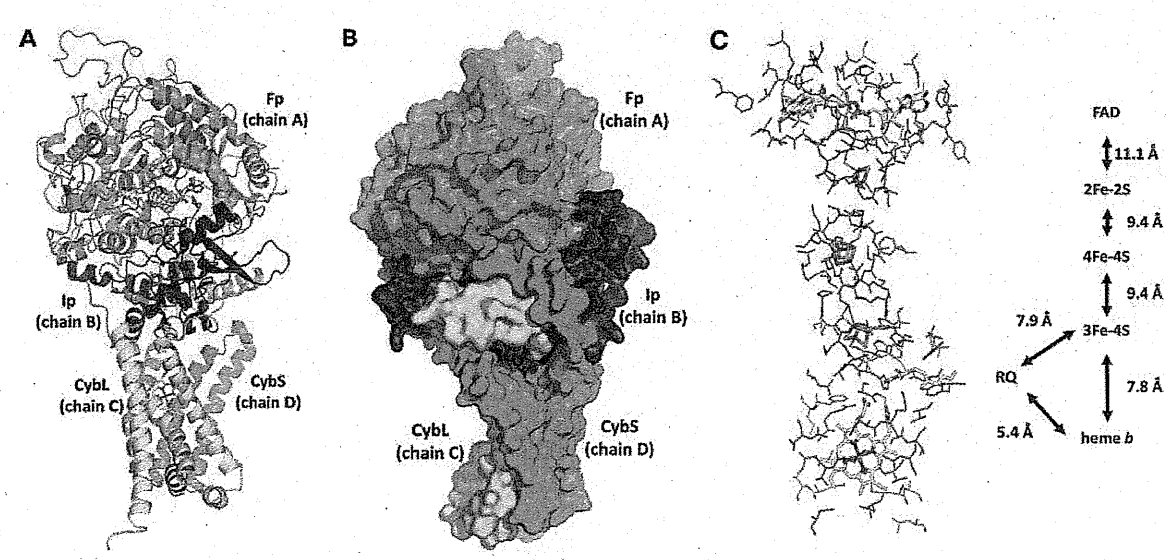

Fig. 1 Structure of *A. suum* QFR. Fp (chain A), Ip (chain B), CybL (chain C) and CybS (chain D) are coloured in green, red, yellow and cyan, respectively. Colour code for each atom type: C (yellow), N (blue), O (red), S (orange) and Fe (brown). (A) Cartoon representation of the *A. suum* QFR structure. FAD, iron–sulphur centres and haem *b* are shown as sticks. (B) Surface model of *A. suum* QFR viewed from a different direction from (A) for easy observation of the extra polypeptide attached to the N-terminus of CybS. (C) The arrangement of FAD, [2Fe–2S], [4Fe–4S], [3Fe–4S], haem *b* and RQ. Their edge-to-edge distances are also shown. Amino acid residues within 5 Å of the prosthetic groups and RQ are shown by a wire model. Conserved residues across amino acid sequences of complex IIs are coloured in magenta.

(Fig. 1A and B) and anchor the *A. suum* QFR to the membrane. A haem *b* is embedded into the interface between the CybL and CybS, and two conserved His residues (His C131 and His D95) are ligated to the haem iron. A distinct cleft, whose location is in agreement with the quinone binding sites proposed for other complex IIs, is formed by Ip, CybL and CybS, and a residual electron density probably revealing a bound RQ is detected in the cleft.

Figure 1C shows the arrangement of the prosthetic groups bound to *A. suum* QFR and their edge-to-edge distances. [2Fe–2S], [4Fe–4S] and [3Fe–4S] line between FAD and RQ as observed in other complex IIs (*15*). Thus, the disposition of the prosthetic groups is critical to allow electron transfer from RQH_2 to FAD via the iron–sulphur centres. The hydrophobic environment around the iron–sulphur centres and distances between neighbouring centres (<14 Å) suggest that the electron transfer from RQH_2 to FAD is carried out by quantum tunneling (*16*), as proposed for *E. coli* SQR (*6*).

Figure 2A shows that fumarate is bound near the FAD isoalloxazine ring in a non-planar conformation. C2, C3 and C4 carboxyl group are in the same plane parallel to the isoalloxazine ring, whereas the C1 carboxyl group is twisted around the C1 and C2 bond with a C3–C2–C1–O1A dihedral angle of 83.7°. The twisting, which is stabilized by hydrogen bonds with Gly A85, Thr A288, Glu A289 and Arg A320, suggests that the uniform distribution of π-electrons over the conjugated double bonds of fumarate is broken and a partial charge separation, $C2^{\delta+}$ and $C3^{\delta-}$, is induced. The contact of $C2^{\delta+}$ with FAD N5 (4.05 Å) suggests that a hydride (or hydride equivalent) is transferred from reduced FAD N5 to $C2^{\delta+}$ in the reduction of fumarate with the reduced FAD. Arg A320 is a probable candidate that supplies a proton to $C3^{\delta-}$ to complete the reduction of fumarate. The twisted conformation of fumarate is also observed in flavoproteins with fumarate reductase acitivity (1D4E, 1P2E, 1QLB and 2E6D), and a similar mechanism is proposed for *E. coli* QFR (*17*) and *Trypanosoma cruzi* dihydroorotate dehydrogenase (*18*).

Figure 2B shows the structure of the RQ binding site proposed for *A. suum* QFR. The site is formed by Ip, CybL and CybS, and is in agreement with ubiquinone binding sites suggested for other complex IIs. [3Fe–4S] is the nearest iron–sulphur centre to RQ (9.2 and 7.9 Å from RQ O1 and RQ O2, respectively), suggesting that electrons are first accepted by [3Fe–4S] upon the oxidization of RQH_2, and then transferred to FAD via [4Fe–4S] and [2Fe–2S].

RQ is surrounded by conserved amino acid residues (Ser C72, Arg C76, Asp D106 and Tyr D107) and is involved in hydrogen bond networks, RQ O1–Tyr D107–Arg C76–Asp D106 and RQ O2–Ser C72–RQ N–Arg C76–Asp D106. Protons abstracted from RQH_2 may leave along these networks. It should be noted that the amino group of RQ, which is replaced by the methoxy group in ubiquinone, is involved in one of the hydrogen bond networks.

In this study, the structure of *A. suum* QFR, the first structure of a mitochondrial QFR-type complex II, has been determined. A comparison of structures of *A. suum* QFR and SQR-type complex II reveals that not only are the protein structures essentially identical to each other, but also the bound prosthetic groups are surrounded by conserved residues (Fig. 1C). Thus, it appears that the bound quinone type plays a role in determining the direction of catalysis, QFR or SQR of complex II. In fact, *A. suum* QFR, which catalyses the reduction of fumarate ($Em' = +30$ mV) by oxidizing RQH_2 ($Em' = -63$ mV) *in vivo*, displays SQR activity,

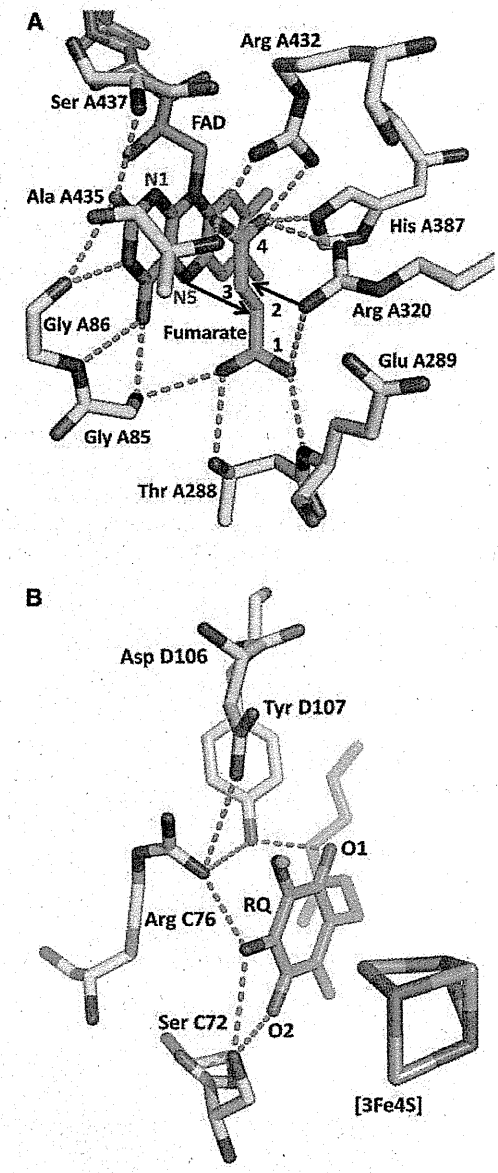

Fig. 2 Close-up views of active site structures of *A. suum* QFR. (A) Fumarate binding site of *A. suum* QFR. The C1 carboxyl group is twisted around the C1 and C2 bond by hydrogen bonds with nearby residues, which induces partial charge separation, $C2^{\delta+}$ and $C3^{\delta-}$. (B) RQH_2 binding site of *A. suum* QFR. Colour code for each atom type: C (yellow), N (blue), O (red), S (orange) and Fe (brown). Fumarate and RQ are coloured in green, FAD in pink. Hydrogen bonds are drawn with cyan dotted lines.

oxidation of succinate ($Em' = +30$ mV), and reduction of ubiquinol ($Em' = +110$ mV) *in vitro*.

The structure also demonstrates a feature unique to *A. suum* QFR. The additional polypeptide composed of 27 residues, which is found only at the N-terminus of *A. suum* CybS, extends to and forms hydrogen bonds with CybL, Ip and Fp (Fig. 1B, cyan), indicating that this unique region probably contributes to the stabilization of the *A. suum* QFR structure. In addition, because no such region has been found in SQR-type complex IIs known to date, this unique feature could make *A. suum* QFR favourable for accepting RQH_2 and fumarate as substrates, although further biochemical and biophysical analyses are necessary to reveal the truth.

Supplementary Data

Supplementary Data are available at *JB* Online.

Funding

This work was supported in part by Creative Scientific Research Grant 18GS0314 (to KK), Grant-in-aid for Scientific Research on Priority Areas 18073004 (to KK) and 19036010 (to SH) from the Japanese Society for the Promotion of Science, and Targeted Proteins Research Program (to KK and SH) from the Japanese Ministry of Education, Science, Culture, Sports and Technology (MEXT).

Conflict of interest

None declared.

References

1. Omura, S., Miyadera, H., Ui, H., Shiomi, K., Yamaguchi, Y., Masuma, R., Nagamitsu, T., Takano, D., Sunazuka, T., Harder, A., Kolbl, H., Namikoshi, M., Miyoshi, H., Sakamoto, K., and Kita, K. (2001) An anthelmintic compound, nafuredin, shows selective inhibition of complex I in helminth mitochondria. *Proc. Natl. Acad. Sci. USA* **98**, 60–62
2. Matsumoto, J., Sakamoto, K., Shinjyo, N., Kido, Y., Yamamoto, N., Yagi, K., Miyoshi, H., Nonaka, N., Katakura, K., Kita, K., and Oku, Y. (2008) Anaerobic NADH-fumarate reductase system is predominant in the respiratory chain of *Echinococcus multilocularis*, providing a novel target for the chemotherapy of alveolar echinococcosis. *Antimicrob. Agents Chemother.* **52**, 164–170
3. Sakai, C., Tomitsuka, E., Esumi, H., Harada, S., and Kita, K. (2012) Mitochondrial fumarate reductase as a target of chemotherapy: from parasites to cancer cells. *Biochim. Biophys. Acta* **1820**, 643–651
4. Sun, F., Huo, X., Zhai, Y., Wang, A., Xu, J., Su, D., Bartlam, M., and Rao, Z. (2005) Crystal structure of mitochondrial respiratory membrane protein complex II. *Cell* **121**, 1043–1057
5. Huang, L.S., Sun, G., Cobessi, D., Wang, A.C., Shen, J.T., Tung, E.Y., Anderson, V.E., and Berry, E.A. (2006) 3-Nitropropionic acid is a suicide inhibitor of mitochondrial respiration that, upon oxidation by complex II, forms a covalent adduct with a catalytic base arginine in the active site of the enzyme. *J. Biol. Chem.* **281**, 5965–5972
6. Yankovskaya, V., Horsefield, R., Tornroth, S., Luna-Chavez, C., Miyoshi, H., Leger, C., Byrne, B., Cecchini, G., and Iwata, S. (2003) Architecture of succinate dehydrogenase and reactive oxygen species generation. *Science* **299**, 700–704
7. Iverson, T.M., Luna-Chavez, C., Cecchini, G., and Rees, D.C. (1999) Structure of the *Escherichia coli* fumarate reductase respiratory complex. *Science* **284**, 1961–1966
8. Lancaster, C.R., Kroger, A., Auer, M., and Michel, H. (1999) Structure of fumarate reductase from *Wolinella succinogenes* at 2.2 Å resolution. *Nature* **402**, 377–385
9. Osanai, A., Harada, S., Sakamoto, K., Shimizu, H., Inaoka, D.K., and Kita, K. (2009) Crystallization of mitochondrial rhodoquinol-fumarate reductase from the parasitic nematode *Ascaris suum* with the specific inhibitor flutolanil. *Acta Crystallogr. Sect. F Struct. Biol. Cryst. Commun.* **65**, 941–944
10. Otwinowski, Z. and Minor, W. (1997) Macromolecular crystallography part A [20] Processing of X-ray diffraction data collected in oscillation mode. *Methods Enzymol.* **276**, 307–326
11. Vagin, A. and Teplyakov, A. (2010) Molecular replacement with *MOLREP*. *Acta Crystallogr. D Biol. Crystallogr.* **66**, 22–25
12. Murshudov, G.N., Vagin, A.A., and Dodson, E.J. (1997) Refinement of macromolecular structures by the maximum-likelihood method. *Acta Crystallogr. D Biol. Crystallogr.* **53**, 240–255
13. Emsley, P. and Cowtan, K. (2004) *Coot*: model-building tools for molecular graphics. *Acta Crystallogr. D Biol. Crystallogr.* **60**, 2126–2132
14. DeLano, W.L. (2002) *The PyMOL Molecular Graphics System*. DeLano Scientific LLC, Palo Alto, California, USA
15. Horsefield, R., Iwata, S., and Byrne, B. (2004) Complex II from a structural perspective. *Curr. Protein Pept. Sci.* **5**, 107–118
16. Page, C.C., Moser, C.C., Chen, X., and Dutton, P.L. (1999) Natural engineering principles of electron tunnelling in biological oxidation-reduction. *Nature* **402**, 47–52
17. Tomasiak, T.M., Archuleta, T.L., Andrell, J., Luna-Chavez, C., Davis, T.A., Sarwar, M., Ham, A.J., McDonald, W.H., Yankovskaya, V., Stern, H.A., Johnston, J.N., Maklashina, E., Cecchini, G., and Iverson, T.M. (2011) Geometric restraint drives on- and off-pathway catalysis by the *Escherichia coli* menaquinol:fumarate reductase. *J. Biol. Chem.* **286**, 3047–3056
18. Inaoka, D.K., Sakamoto, K., Shimizu, H., Shiba, T., Kurisu, G., Nara, T., Aoki, T., Kita, K., and Harada, S. (2008) Structures of *Trypanosoma cruzi* dihydroorotate dehydrogenase complexed with substrates and products: atomic resolution insights into mechanisms of dihydroorotate oxidation and fumarate reduction. *Biochemistry* **47**, 10881–10891

Structure of the trypanosome cyanide-insensitive alternative oxidase

Tomoo Shiba[a,1,2], Yasutoshi Kido[a,1,3], Kimitoshi Sakamoto[a,4], Daniel Ken Inaoka[a], Chiaki Tsuge[a], Ryoko Tatsumi[a], Gen Takahashi[b], Emmanuel Oluwadare Balogun[a,b,c], Takeshi Nara[d], Takashi Aoki[d], Teruki Honma[e], Akiko Tanaka[e], Masayuki Inoue[f], Shigeru Matsuoka[f], Hiroyuki Saimoto[g], Anthony L. Moore[h], Shigeharu Harada[b,5], and Kiyoshi Kita[a,5]

[a]Department of Biomedical Chemistry, Graduate School of Medicine, and [f]Graduate School of Pharmaceutical Sciences, The University of Tokyo, Tokyo 113-0033, Japan; [b]Department of Applied Biology, Graduate School of Science and Technology, Kyoto Institute of Technology, Kyoto 606-8585, Japan; [c]Department of Biochemistry, Ahmadu Bello University, Zaria 2222, Nigeria; [d]Department of Molecular and Cellular Parasitology, Juntendo University School of Medicine, Tokyo 113-8421, Japan; [e]Systems and Structural Biology Center, RIKEN, Tsurumi, Yokohama 230-0045, Japan; [g]Department of Chemistry and Biotechnology, Graduate School of Engineering, Tottori University, Tottori 680-8552, Japan; and [h]Biochemistry and Molecular Biology, School of Life Sciences, University of Sussex, Brighton BN1 9QG, United Kingdom

Edited[†] by John E. Walker, Medical Research Council Mitochondrial Biology Unit, Cambridge, United Kingdom, and approved February 11, 2013 (received for review October 23, 2012)

In addition to haem copper oxidases, all higher plants, some algae, yeasts, molds, metazoans, and pathogenic microorganisms such as *Trypanosoma brucei* contain an additional terminal oxidase, the cyanide-insensitive alternative oxidase (AOX). AOX is a diiron carboxylate protein that catalyzes the four-electron reduction of dioxygen to water by ubiquinol. In *T. brucei*, a parasite that causes human African sleeping sickness, AOX plays a critical role in the survival of the parasite in its bloodstream form. Because AOX is absent from mammals, this protein represents a unique and promising therapeutic target. Despite its bioenergetic and medical importance, however, structural features of any AOX are yet to be elucidated. Here we report crystal structures of the trypanosomal alternative oxidase in the absence and presence of ascofuranone derivatives. All structures reveal that the oxidase is a homodimer with the nonhaem diiron carboxylate active site buried within a four-helix bundle. Unusually, the active site is ligated solely by four glutamate residues in its oxidized inhibitor-free state; however, inhibitor binding induces the ligation of a histidine residue. A highly conserved Tyr220 is within 4 Å of the active site and is critical for catalytic activity. All structures also reveal that there are two hydrophobic cavities per monomer. Both inhibitors bind to one cavity within 4 Å and 5 Å of the active site and Tyr220, respectively. A second cavity interacts with the inhibitor-binding cavity at the diiron center. We suggest that both cavities bind ubiquinol and along with Tyr220 are required for the catalytic cycle for O_2 reduction.

diiron protein | neglected tropical diseases | monotopic membrane protein | drug target | ubiquinol oxidase

The alternative oxidase (AOX) is a nonprotonmotive ubiquinol oxidase catalyzing the four-electron reduction of dioxygen to water (1). The gene encoding this protein has been found in all higher plants, some algae, yeast, slime molds, free-living amoebae, eubacteria, nematodes, and some parasites including *Trypanosoma brucei* (2–5). *T. brucei* is a parasite that causes human African sleeping sickness and nagana in livestock and is transmitted by the tsetse fly (5). The development of chemotherapy and the continued search for new, unique therapeutic targets for African trypanosomiasis are urgently required, because current treatments, which are poorly targeted, have unacceptable side effects and efficacy (6).

The bloodstream form of *T. brucei* is equipped with a unique energy metabolism, namely an altered respiratory chain (5) and a modified ATP synthase (7). The parasites live as the bloodstream form in the mammalian host and as the procyclic form in the tsetse fly (5). The procyclic form of *T. brucei* contains a cytochrome-dependent respiratory chain in addition to an alternative oxidase, whereas within the bloodstream trypanosomes use the glycolytic pathway, localized in the glycosome, as their major source of ATP (5, 8). Once the parasites invade the mammalian host in the bloodstream, both the cytochrome respiratory pathway and oxidative phosphorylation disappear and are replaced by the trypanosomal alternative oxidase (TAO), which functions as the sole terminal oxidase to reoxidize NADH accumulated during glycolysis (5). Because NADH reoxidation is essential for parasite survival and mammalian hosts do not possess this protein, TAO is considered to be a unique target for antitrypanosomal drugs (9). Indeed, we have previously reported that the antibiotic ascofuranone (AF), isolated from the pathogenic fungus *Ascochyta viciae*, specifically inhibits the quinol oxidase activity of TAO at subnanomolar concentrations and rapidly kills the parasites (10). Furthermore, we have confirmed the chemotherapeutic efficacy of ascofuranone in vivo (11, 12).

Despite universal conservation of the gene encoding the AOX and diversified physiology (2), the molecular features of this protein have yet to be fully characterized. Current structural models predict that the AOX is an integral interfacial membrane protein that interacts with a single leaflet of the lipid bilayer and contains a nonhaem diiron carboxylate active site (1, 13, 14). This model is supported by extensive site-directed mutagenesis and spectroscopic studies (3, 15–20).

There are many proteins that belong to the diiron carboxylate protein family, and in each case they are characterized by the possession of two copies of the diiron binding motifs (21, 22). To date the majority of proteins within this family whose crystal structures have been determined are soluble proteins, and hence determination of a crystal structure of a member of the membrane-bound class is vital, because it would transformationally improve our understanding of the structure–function relationships of this functionally diverse family of proteins. In this paper we report on the crystal structure of the

Author contributions: T.S., Y.K., K.S., D.K.I., E.O.B., A.L.M., S.H., and K.K. designed research; T.S., Y.K., D.K.I., C.T., R.T., G.T., E.O.B., and H.S. performed research; K.S. and H.S. contributed new reagents/analytic tools; T.S., Y.K., G.T., T.N., T.A., T.H., A.T., M.I., and S.M. analyzed data; and T.S., Y.K., A.L.M., S.H., and K.K. wrote the paper.

The authors declare no conflict of interest.

[†]This Direct Submission article had a prearranged editor.

Data deposition: The atomic coordinates and structure factors have been deposited in the Protein Data Bank, www.pdb.org (PDB ID codes 3VV9 [trypanosomal alternative oxidase (TAO)], 3VVA [TAO-AF2779OH complex], and 3W54 [TAO-colletochlorin B complex]).

[1]T.S. and Y.K. contributed equally to this work.

[2]Present address: Department of Applied Biology, Graduate School of Science and Technology, Kyoto Institute of Technology, Kyoto 606-8585, Japan.

[3]Present address: Division of International Health, Oita University Faculty of Medicine, Yufu, Oita 879-5593, Japan.

[4]Present address: Faculty of Agriculture and Life Science, Hirosaki University, Hirosaki 036-8561, Japan.

[5]To whom correspondence may be addressed. E-mail: harada@kit.ac.jp or kitak@m.u-tokyo.ac.jp.

This article contains supporting information online at www.pnas.org/lookup/suppl/doi:10.1073/pnas.1218386110/-/DCSupplemental.

oxidized form of the trypanosomal alternative oxidase at 2.85 Å. In addition to this very important milestone we also describe the structures of the active site of the enzyme in the presence of AF derivatives, AF2779OH and colletochlorin B (CCB), at 2.6 Å and 2.3 Å resolution, respectively. We believe that a detailed knowledge of the active site of the enzyme in the presence of such inhibitors will lead to a greater rational design of further potent and safer antitrypanosomal drugs.

Results and Discussion

Overall Structure of TAO. We have recently established protocols to prepare highly purified and stable TAO, which has enabled us to crystallize the enzyme (23, 24). The crystal structure of TAO determined at 2.85 Å resolution (*SI Appendix*, Table S1) contains four monomers per asymmetric unit that associate to form homodimers (Fig. 1*A* and *SI Appendix*, Fig. S1*A*). Each monomer, which lacks about 30 residues in both N- and C-terminal regions due to faint electron density, consists of a long N-terminal arm, six long α helices (α1–α6), and four short helices (S1–S4). The long helices are arranged in an antiparallel fashion with α2, α3, α5, and α6 forming a four-helix bundle that accommodates a diiron center, as widely observed in other diiron carboxylate proteins (1, 14) (*SI Appendix*, Fig. S2). Except for the N-terminal arm, each monomer is shaped as a compact cylinder (50 × 35 × 30 Å), and there are no significant structural differences among monomers in the asymmetric unit, as indicated by rms deviations (0.49~0.68 Å) for superimposed Cα positions of the six helices calculated between a pair of monomers. However, loops connecting adjacent helices show larger differences among monomers, resulting in somewhat larger rms deviations (0.67~0.88 Å) when calculated using all Cα atoms.

In the dimer, two monomers are related by a noncrystallographic twofold axis approximately perpendicular to the bundle (Fig. 1*A*). Helices α2, α3, and α4 of one monomer and α2*, α3*, and α4* of the other (asterisk denotes helix of a neighboring monomer) build a dimer interface, where six completely conserved residues (H138, L142, R143, R163, L166, and Q187) and 12 highly conserved residues (M131, M135, L139, S141, M145, R147, D148, L156, A159, M167, R180, and I183) are involved in the interaction between monomers (*SI Appendix*, Fig. S3), suggesting that a dimeric structure is common to all AOXs. In addition, the N-terminal arm (P31~R62) of one monomer extends into the other monomer (Fig. 1*A*), suggesting that the arm is important for dimerization. Upon dimerization, about 2,490 Å^2 of solvent-accessible surface (35% of the total dimer surface) is buried. A large hydrophobic region is visible on one side of the dimer surface that is formed by α1 and α4 plus the C-terminal region of α2 and the N-terminal region of α5 from both monomers (Fig. 1*B Left*). Because the opposite side of the dimer surface is relatively hydrophilic (Fig. 1*B Right*), we propose that the dimer is bound to the mitochondrial inner membrane via this hydrophobic region in an interfacial fashion, as originally suggested by Andersson and Nordlund (13). The membrane penetration depth of TAO, calculated by PPM web server (25), is 8.4 Å, roughly corresponding to the radius of a helix. In addition, basic residues (R106, R143, R180, R203, and R207) are distributed along a boundary between the hydrophobic and hydrophilic regions of the dimer surface (Fig. 1*C* and *SI Appendix*, Fig. S4). They are conserved across all amino acid sequences of the membrane-bound AOXs shown in *SI Appendix*, Fig. S5, and their locations make these residues ideal candidates to interact with the negatively charged phospholipids head groups of membranes.

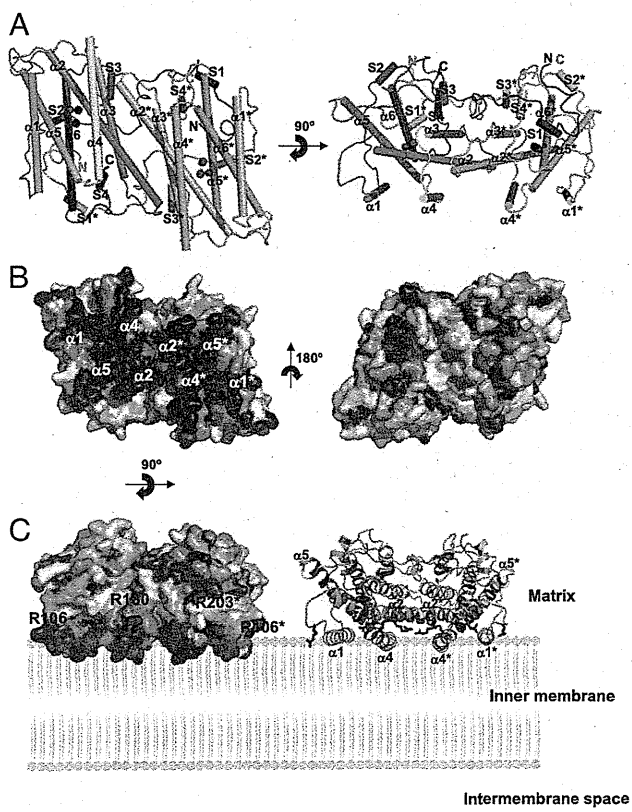

Fig. 1. Structure of TAO. Long helices are labeled α1 to α6 and short ones S1 to S4. Diiron and hydroxo atoms are shown as magenta spheres. (*A*) Dimeric structure of TAO viewed roughly perpendicular (*Left*) and parallel (*Right*) to the helix axes. Helices are shown as cylinders. Chain A is colored in rainbow from blue (N terminus) to red (C terminus) and chain B in pink. (*B*) Surface representation of the TAO dimer showing the hydrophobic (*Left*) and hydrophilic (*Right*) surfaces. Colors are according to the following hydrophobicity scale: red, high hydrophobicity; white, low hydrophobicity (www.pymolwiki.org/index.php/Color_h). (*C*) Proposed binding model of the TAO dimer to membranes shown by surface (*Left*) and cartoon (*Right*) representations. The hydrophobic region on the molecular surface of the TAO dimer faces the membrane. Conserved basic amino acid residues, which are distributed along a boundary between the hydrophobic and hydrophilic regions of the dimer surface, are colored in blue. Residue names are labeled in black (asterisk denotes in chain B).

Structure of Diiron Active Site. The structure of the diiron active site was refined as an oxidized Fe(III)-Fe(III) form with a single hydroxo-bridge (Fig. 2 and *SI Appendix*, Fig. S6), as previously predicted from spectroscopic studies (19, 20). The active site, which is located in a hydrophobic environment deep inside the TAO molecule, is composed of the diiron center and four glutamate (E123, E162, E213, and E266) and two histidine residues (H165 and H269), all of which are completely conserved (*SI Appendix*, Fig. S5). In addition, the conserved hydrophobic residues (L122, A126, L212, A216, Y220, and I262) are within 6 Å of the diiron center (Fig. 2*A*). The average Fe1–Fe2 distance of the four monomers in the asymmetric unit is 3.3 ± 0.2 Å and, in addition to the hydroxo-bridge, Fe1 and Fe2 are bridged by E162 and E266 and furthermore coordinated in a bidentate fashion by E123 and E213, respectively, thereby resulting in a five-coordinated diiron center possessing a distorted square pyramidal geometry (Fig. 2*B* and *SI Appendix*, Fig. S6 and Table S2). The most striking feature of the diiron active site in the oxidized state is that, as predicted from our earlier FTIR studies (26), histidine residues (H165 and H269) are too distant from both Fe1 and Fe2 (H165: 3.3~4.0 Å, H269: 3.8~4.4 Å) to coordinate to the diiron center. They do, however, form hydrogen bonds with E123, N161, E162, E213, and D265. N161 and D265 are situated in the center of the hydrogen-bond network and extend the network to W65, Y246, and W247. These residues, apart from W65, are again completely conserved (*SI Appendix*, Fig. S5), suggesting that the hydrogen bond network is important for the stabilization of the AOX active site. To our knowledge, TAO is the only structure of

BIOCHEMISTRY

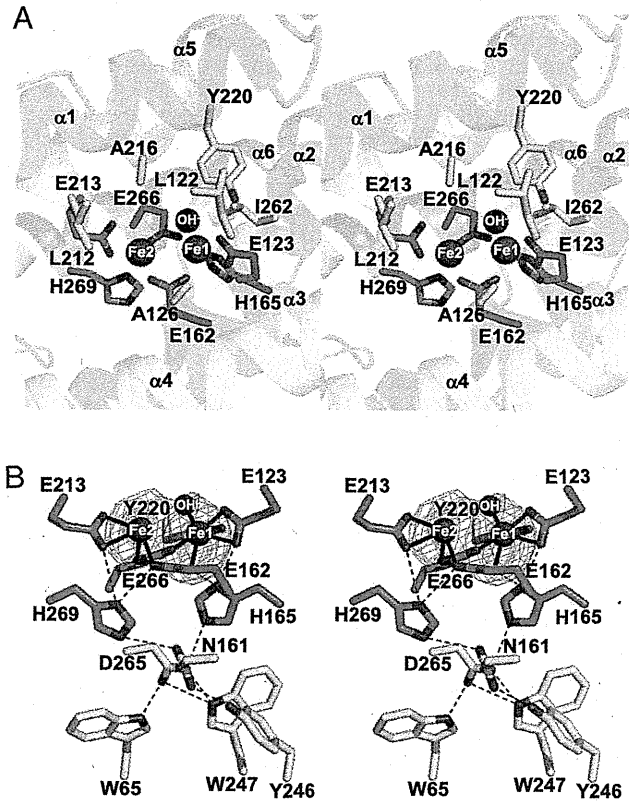

Fig. 2. Diiron structure of TAO. (*A*) Stereo view of the diiron active site and its environment. Diiron and hydroxo atoms are shown as magenta spheres, four glutamate and two histidine residues important for diiron binding as green sticks, neighboring residues within 6 Å of the diiron in yellow, nitrogen in blue, and oxygen in red. (*B*) Stereo view of the coordinate bonds (solid lines) and hydrogen bonds (dashed lines) of the diiron active site. Sigma-A weighted electron density map calculated from the refined model of the ligand-free TAO with the diiron centers omitted from the phase calculation is also shown. Contour levels are 1.0 σ (blue) and 3.0 σ (orange). H165 forms hydrogen bonds with E123, E162, and N161 and H269 with E162, E213, and N161. N161, which is situated in the center of the hydrogen network, forms additional hydrogen bonds with Y246 and D265. D265 forms hydrogen bonds with W65 and W247.

an oxidized diiron active site that is ligated solely by carboxylate ligands. In contrast, diiron active sites of soluble diiron proteins with known structures, Δ^4 ACP desaturase (27) (PDB ID code 2UW1), methane monooxygenase (28) (PDB ID code 1MMO), rubrerythrin (29) (PDB ID code 1LKM), and ribonucleotide reductase R2 subunit (30) (PDB ID code 1RIB), are all coordinated by at least one if not two histidine residues.

Important Tyrosine Residues. Similar to ribonucleotide reductase, tyrosine residues have also been proposed to play an essential role in the catalytic cycle of AOX (1, 31, 32). Scrutiny of *SI Appendix*, Fig. S5 reveals that although there seem to be four conserved tyrosine residues (Y198, Y211, Y220, and Y246), only three of which (not Y211) are totally conserved across all amino acid sequences of membrane-bound AOXs, including the plastid AOX (33), Y220 is buried deep within the four-helix bundle and within 4 Å of the diiron center (Fig. 2*A*), making it the most likely candidate for the amino acid radical involved in the catalytic cycle (32). Indeed, Y220 is absolutely conserved across all AOXs sequenced to date, and mutational analyses have unequivocally demonstrated that this residue is critical for enzymatic activity of all AOXs (1, 33). Y198 has been proposed to be involved in ubiquinol binding, although its mutation does not lead to the complete loss of activity (18, 34). The crystal structure of TAO (*SI Appendix*, Fig. S7) indicates that Y198, located on the C-terminal portion of helix α4, is separated by more than 15 Å from the diiron center and forms a hydrogen bond with a conserved H206 protruding from the N-terminal portion of helix α5. Such a position suggests it probably stabilizes the structure of TAO rather than being directly involved in ubiquinol binding. Although Y246 on helix S3 is located 10.7 ± 0.2 Å from the diiron center, which is within electron tunneling distance [<14 Å (35)], it is more likely to be involved in the hydrogen-bonding network rather than electron transport, because it is 2.9 ± 0.2 Å from N161 in helix α3 (Fig. 2*B* and *SI Appendix*, Fig. S7). This notion is supported by the result that a Y246A mutant retains some activity (1, 34), which would not be the case if it were essential for electron transfer.

Binding Mode of the Potent Inhibitor AF2779OH. Until recently little structural information was available on the mode of AF binding to TAO, even given its specificity. Inhibitor kinetic studies indicated that AF showed a mixed-type inhibition against ubiquinol (23), suggesting that the ring moiety and the geranyl portions of AF are important for the interaction of the inhibitor with TAO. To investigate whether this was the case, an AF derivative lacking the furanone ring was synthesized (AF2779OH: 5-chloro-3-[(2*E*,6*E*)-8-hydroxy-3,7-dimethylnona-2,6-dienyl]-2,4-dihydroxy-6-methylbenzaldehyde; Fig. 3*A*). AF2779OH possesses similar inhibitory properties (IC_{50} = 0.48 nM for TAO; minimum inhibitory concentration = 30 nM for *T. brucei brucei*) to AF, indicating that the furanone ring is indeed not critical for inhibitory activity, thereby rendering it useful to determine the location of AF binding to TAO. A crystal of the TAO–AF2779OH complex was prepared by soaking in the cryoprotectant solution supplemented with the inhibitor and the structure determined at 2.6 Å by molecular replacement using the inhibitor-free TAO structure as a template (*SI Appendix*, Table S1 and Fig. S1*B*). In addition, the crystal structure of TAO complexed with CCB, another AF derivative (5-chloro-3-[(2E)-3,7-dimethylocta-2,6-dienyl]-2,4-dihydroxy-6-methylbenzaldehyde), was also determined at 2.3 Å resolution (*SI Appendix*, Table S1 and Fig. S1*C*). *SI Appendix*, Figs. S8 and S9 show that CCB is bound to the enzyme in a manner similar to AF2779OH. CCB also strongly inhibits TAO (IC_{50} = 0.20 nM for TAO); however, unlike AF and AF2779OH, it is toxic to mice. Given the toxicity of CCB we will therefore focus further discussion on the structure of TAO complexed with AF2779OH, because it is a safer drug candidate for trypanosomiasis.

Fig. 3 *B* and *C* show the dimeric structure of the TAO–AF2779OH complex and residues around the bound AF2779OH, respectively. The binding cavity of AF2779OH is located near the membrane surface between helices α1 and α4 and is lined by 16 highly conserved residues (V92, R96, F99, R118, C119, F121, L122, E123, V125, M190, L212, E213, E215, A216, T219, and Y220) plus C95 (Fig. 3*C* and *SI Appendix*, Figs. S5 and S8 and Table S3). It is also apparent from Fig. 3*C* and *SI Appendix*, Fig. S8 and Table S3 that the aromatic head of AF2779OH is located close to the diiron active site and the C2–OH forms hydrogen bonds with R118 and T219. In addition, the aldehyde oxygen at the C1 position interacts with E123 through a hydrogen bond network, C1–CH = O···C119–SH···Y220–OH···E123–COO^-, in the B and D subunit, whereas the aldehyde oxygens of the A and C subunits form an intrasubunit hydrogen bond with C2–OH. These hydrogen bonds are also observed in the TAO–CCB complex and seem to be important for the potent inhibitory activities of both inhibitors. Indeed, IC_{50} values of AF derivatives lacking this aldehyde group (K2-9 and K4-9 in *SI Appendix*, Fig. S10) increase substantially (36). It is also likely that van der Waals contacts formed between AF2779OH and TAO (*SI Appendix*, Table S3) contribute to the potent effect of these inhibitors (36). In the inhibited enzymes the distances between H165 and Fe1 (2.3 ± 0.1 and 2.4 ± 0.1 Å for AF2779OH and CCB, respectively) are shorter than that observed in the inhibitor-free structure (3.5 ± 0.3 Å), and hence H165 can now